Two-loop Bhabha scattering in QED: Vertex and one-loop by one-loop contributions

R. Bonciani* and A. Ferroglia†

Fakultät für Mathematik und Physik, Albert-Ludwigs-Universität Freiburg, D-79104 Freiburg, Germany

(Received 11 July 2005; published 22 September 2005)

In the context of pure QED, we obtain analytic expressions for the contributions to the Bhabha scattering differential cross section at order α^4, which originate from the interference of two-loop photonic vertices with tree-level diagrams and from the interference of one-loop photonic diagrams amongst themselves. The ultraviolet renormalization is carried out. The IR-divergent soft-photon emission corrections are evaluated and added to the virtual cross section. The cross section obtained in this manner is valid for on-shell electrons and positrons of finite mass and for arbitrary values of the center of mass energy and momentum transfer. We provide the expansion of our results in powers of the electron mass, and we compare them with the corresponding expansion of the complete order α^4 photonic cross section, recently obtained by A. A. Penin [Phys. Rev. Lett. **95**, 010408 (2005).]. As a by-product, we obtain the contribution to the Bhabha scattering differential cross section of the interference of the two-loop photonic boxes with the tree-level diagrams, up to terms suppressed by positive powers of the electron mass. We evaluate numerically the various contributions to the cross section, paying particular attention to the comparison between exact and expanded results.

DOI: 10.1103/PhysRevD.72.056004 PACS numbers: 11.15.Bt, 12.20.Ds

I. INTRODUCTION

The Bhabha scattering process plays a crucial role in the study of elementary particle phenomenology, since it is the process employed in the luminosity measurement at e^+e^- colliders. The small-angle Bhabha scattering at high (~ 100 GeV) center of mass energy and the large-angle Bhabha scattering at intermediate (1–10 GeV) energies have cross sections that are large and QED dominated; these two characteristics allow for precise experimental measurements, as well as for a detailed theoretical evaluation of the cross section.

The radiative corrections to the Bhabha scattering in pure QED have been extensively studied (see [1], and references therein). The $\mathcal{O}(\alpha^3)$ corrections have been known for a long time, even in the full electroweak standard model [2]. The second order QED corrections $\mathcal{O}(\alpha^4)$ were the subject of renewed interest in the past few years, and several works have been devoted to the study of second order radiative corrections, both virtual and real, enhanced by factors of $\ln^n(s/m^2)$ (with $n = 1, 2$, s the c.m. energy, and m the mass of the electron) [3–5]. The complete set of these corrections was finally obtained in Ref. [6] by employing the QED virtual corrections for massless electron and positrons of Ref. [7], the results of Ref. [8], and by using the known structure of the IR poles in dimensional regularization [9]. Very recently, the complete set of photonic $\mathcal{O}(\alpha^4)$ corrections to the cross section that are not suppressed by positive powers of the ratio m^2/s were obtained in Ref. [10]. The subset of virtual corrections of $\mathcal{O}(\alpha^4)$ involving a closed fermion loop, together with the corresponding soft-photon emission corrections, were obtained in an analytic and nonapproximated form in Refs. [11–13]. The results contained in these papers do not rely on any mass expansion, and they are valid for arbitrary values of the c.m. energy s, momentum transfer t, and electron mass m. In Refs. [11–13], the calculation of the relevant loop diagrams was performed by employing the Laporta-Remiddi algorithm [14], which takes advantage of the integration by parts [15] and Lorentz-invariance [16] identities in order to reduce the problem to the calculation of a small set of master integrals. The master integrals are calculated using the differential equations method [17]; their expression is given in terms of harmonic polylogarithms (HPLs) [18]. Both IR and UV divergencies were regularized in the dimensional regularization scheme [19] and they appear, in the intermediate results, as singularities in $(D - 4)$, where D is the dimension of the spacetime. It is natural to apply the same approach to the calculation of the complete set of $\mathcal{O}(\alpha^4)$ virtual corrections. At present, the list of the master integrals required to complete the calculation is available in Refs. [20,21]. However, only very few of the master integrals related to the two-loop photonic box diagrams have thus far been calculated [20–22]. The subset of second order radiative corrections due to the interference of one-loop diagrams was studied in Ref. [23].

In using the results of Refs. [24,25], we calculate in this paper the following $\mathcal{O}(\alpha^4)$ corrections to the differential cross section in QED:

(i) corrections due to the interference of the two-loop photonic vertex diagrams with the tree-level amplitude;
(ii) corrections due to the interference of one-loop photonic diagrams amongst themselves;

*Electronic address: Roberto.Bonciani@physik.uni-freiburg.de
†Electronic address: Andrea.Ferroglia@physik.uni-freiburg.de

(iii) corrections due to the emission of two real soft photons from a tree-level diagram and of one soft photon from a one-loop photonic diagram.

These three classes of diagrams provide separately gauge independent contributions to the cross section.[1] All of the contributions mentioned above are calculated for finite electron mass and for arbitrary values of the c.m. energy s and momentum transfer t. We employ dimensional regularization in order to regularize both UV and IR divergencies. The UV renormalization is carried out in the on-shell scheme. By following the same technique of Ref. [13], we pair virtual and soft-photon emission corrections in order to check the cancellation of the IR singularities. Our results contain residual IR poles; we discuss their origin and their cancellation against corresponding terms arising from the two-loop photonic graphs.

We also expand our results, which retain the full dependence on the electron mass, in the limit in which the electron mass is negligible with respect to the Mandelstam invariants. In this way, it is possible:

(i) to prove that our results reproduce the correct small-angle Bhabha scattering cross section at $\mathcal{O}(\alpha^4)$, which is determined by the Dirac vertex form factor only [4];
(ii) to provide strong cross-checks of a large part of the result of Ref. [10];
(iii) to find, by subtracting our result from the cross section of Ref. [10], the contribution to the cross section of the interference between two-loop photonic boxes and the tree-level amplitude;
(iv) to investigate the numerical relevance of the terms suppressed by positive powers of the electron mass.

This paper is structured as follows: After a brief summary of our notation in Sec. II, in Sec. III we discuss the irreducible two-loop vertex photonic corrections, providing an expression for their contribution to the virtual differential cross section. In Secs. IV, V, and VI, we calculate the interference of the reducible vertex diagrams with the tree-level amplitude, the interference of the one-loop vertex diagrams with themselves and with the one-loop box diagrams, respectively, and we obtain the corresponding contributions to the virtual differential cross section. In Sec. VII, we complete the analysis of the interference amongst one-loop diagrams by considering the interference of one-loop boxes. In Sec. VIII, we discuss the soft-photon emission at $\mathcal{O}(\alpha^4)$, and, in Sec. IX, we explicitly show how the cancellation of the IR divergencies works between virtual and soft corrections. In Sec. X, we analyze the expansion of our results in the limit $m^2/s \to 0$; we discuss the behavior of the cross section at small angle, compare our calculations with the results present in the literature, and discuss the numerical accuracy of the expansion. Section XI contains our conclusions. In Appendix A, we collect the definition of some functions introduced in the paper. Finally, in Appendix B, we provide the expressions of the contribution of the two-loop photonic boxes to the differential cross section at order α^4 in the limit $m^2/s \to 0$; all of the functions of the Mandelstam variables introduced and employed throughout the paper are available in electronic format in Ref. [26].

[1]The partial results presented in the following sections are obtained by performing the calculations in the Feynman gauge.

II. KINEMATIC NOTATION AND CONVENTIONS

In this paper, we employ the notation and conventions adopted in Refs. [11–13], which are summarized in the present section. We consider the Bhabha scattering process:

$$e^-(p_1) + e^+(p_2) \to e^-(p_3) + e^+(p_4), \tag{1}$$

where p_1, p_2, p_3, and p_4 are the momenta of the incoming electron, incoming positron, outgoing electron, and outgoing positron, respectively. All of the external particles are on their mass shell, i.e. $p_i^2 = -m^2$ $(i = 1, \ldots, 4)$, where m is the electron mass.

The Mandelstam invariants s, t, and u are related to the beam energy (E) and scattering angle in the center of mass frame of reference (θ) by the relations

$$s \equiv -P^2 \equiv -(p_1 + p_2)^2 = 4E^2, \tag{2}$$

$$t \equiv -Q^2 \equiv -(p_1 - p_3)^2 = -4(E^2 - m^2)\sin^2\frac{\theta}{2}, \tag{3}$$

$$u \equiv -V^2 \equiv -(p_1 - p_4)^2 = -4(E^2 - m^2)\cos^2\frac{\theta}{2}. \tag{4}$$

Moreover, the Mandelstam invariants satisfy the relation $s + t + u = 4m^2$.

The analytic expressions for the vertex and box form factors that we employ in the rest of the paper are calculated in the nonphysical kinematic region $s < 0$ and are then analytically continued to the physical region $s > 4m^2$. In order to express the results (for $s < 0$) in a compact form, it is convenient to introduce the dimensionless variables x, y, and z, defined through the following relations:

$$s \equiv -m^2\frac{(1-x)^2}{x}, \qquad x = \frac{\sqrt{4m^2 - s} - \sqrt{-s}}{\sqrt{4m^2 - s} + \sqrt{-s}}, \qquad 0 \le x \le 1, \tag{5}$$

$$t \equiv -m^2\frac{(1-y)^2}{y}, \qquad y = \frac{\sqrt{4m^2 - t} - \sqrt{-t}}{\sqrt{4m^2 - t} + \sqrt{-t}}, \qquad 0 \le y \le 1, \tag{6}$$

$$u \equiv -m^2 \frac{(1-z)^2}{z}, \qquad z = \frac{\sqrt{4m^2-u}-\sqrt{-u}}{\sqrt{4m^2-u}+\sqrt{-u}}, \tag{7}$$

$0 \le z \le 1$.

The analytic continuation of all the form factors to the physical region $s > 4m^2$ can be readily obtained by replacing $x \to -x' + i\epsilon$, where ϵ is an infinitesimal positive quantity and where

$$x' = -\frac{\sqrt{s-4m^2}-\sqrt{s}}{\sqrt{s-4m^2}+\sqrt{s}}, \tag{8}$$

(see [12] for a more detailed discussion).

The Bhabha scattering differential cross section, calculated by summing over the spins of the final state and averaged over the spins of the initial one, can be expanded in powers of the fine structure constant α as follows:

$$\frac{d\sigma(s,t,m^2)}{d\Omega} = \frac{d\sigma_0(s,t,m^2)}{d\Omega} + \sum_{i=V,S}\left[\left(\frac{\alpha}{\pi}\right)\frac{d\sigma_1^{(i)}(s,t,m^2)}{d\Omega} + \left(\frac{\alpha}{\pi}\right)^2 \frac{d\sigma_2^{(i)}(s,t,m^2)}{d\Omega}\right], \tag{9}$$

where the superscripts V and S indicate virtual and soft-photon emission contributions, respectively, while the subscripts 0, 1, and 2 label the tree-level, $\mathcal{O}(\alpha^3)$, and $\mathcal{O}(\alpha^4)$ corrections, respectively.

The tree-level [$\mathcal{O}(\alpha^2)$] and $\mathcal{O}(\alpha^3)$ corrections are well known (their explicit expressions are collected, for example, in Refs. [12,13]). The contribution of $\mathcal{O}(\alpha^4)$ to the virtual cross section can be further split as follows:

$$\begin{aligned}\frac{d\sigma_2^{(V)}(s,t,m^2)}{d\Omega} &= \frac{d\sigma_2^{(V,\text{ph Boxes})}(s,t,m^2)}{d\Omega} \\ &+ \frac{d\sigma_2^{(V,\text{ph Vertices})}(s,t,m^2)}{d\Omega} \\ &+ \frac{d\sigma_2^{(V,N_F=1)}(s,t,m^2)}{d\Omega},\end{aligned} \tag{10}$$

where the superscript $N_F = 1$ indicates the UV-renormalized diagrams including a closed fermion loop (calculated, together with the corresponding soft-radiation diagrams, in Refs. [12,13]). The superscript "ph Vertices" indicates the contribution of all of the UV-renormalized photonic corrections which include at least one vertex diagram, while the superscript "ph Boxes" indicates the contribution to the cross section of the photonic corrections which include box diagrams only.

This paper is dedicated to the calculation of $d\sigma_2^{(V,\text{ph Vertices})}/d\Omega$, as well as to the calculation of the contribution to $d\sigma_2^{(V,\text{ph Boxes})}/d\Omega$ deriving from the interference of one-loop box diagrams amongst themselves; the soft-photon emission corrections that cancel the residual IR poles in the quantities mentioned above are also discussed. By employing these results and the findings of Ref. [10], we also obtain the contribution of the interference of the two-loop photonic boxes to the cross section at order α^4, up to terms of order m^2/s excluded.

III. IRREDUCIBLE TWO-LOOP VERTEX CORRECTIONS

In this section, we obtain the contribution of the irreducible photonic vertex corrections to the Bhabha scattering differential cross section at order α^4. Four of the two-loop irreducible vertex graphs, which correct the electron current in the t-channel photon-exchange contribution to the Bhabha scattering, are shown in Fig. 1. There are two other graphs contributing to the process: these are the mirror images of diagrams 1(c) and 1(d) with the fermionic arrow reversed, and their contribution to the differential cross section is identical to that of the diagrams in 1(c) and 1(d). We explicitly checked that the sum of the graphs 1(a) and 1(b) and of the graphs 1(c) and 1(d) are separately gauge independent in the class of the covariant linear gauges.

The explicit expressions of diagrams 1(a)–1(d) were calculated in Ref. [25]. The electron current which includes the two-loop photonic corrections can be written as

$$\begin{aligned}\Gamma^\mu(p_1,p_3) = \left(\frac{\alpha}{\pi}\right)^2\Bigg[& F_1^{(2l,\text{ph})}(t)\gamma^\mu \\ & + \frac{1}{2m}F_2^{(2l,\text{ph})}(t)\sigma^{\mu\nu}(p_1-p_3)\Bigg],\end{aligned} \tag{11}$$

where $\sigma^{\mu\nu} = -i/2[\gamma^\mu, \gamma^\nu]$. The electron spinors and the dependence of the form factors $F_i^{(2l,\text{ph})}(t)$ $(i = 1, 2)$ on the electron mass m are omitted in Eq. (11). The expression of the contribution of the single diagrams to the UV-renormalized form factors $F_i^{(2l,\text{ph})}(t)$ can be found in Refs. [25,26]. The form factors shown in Eq. (11) still include IR singularities, which are regularized within the dimensional regularization scheme. The Laurent expansion of the form factors is

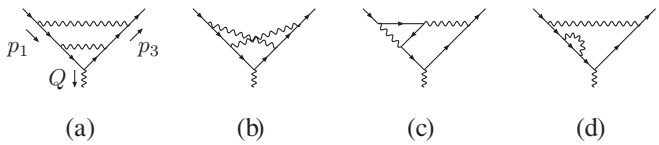

FIG. 1. Two-loop irreducible diagrams contributing to the photonic vertex corrections of the electron current in the t channel. The two diagrams, analogous to (c) and (d), which have an insertion of a one-loop vertex or a self-energy correction on the outgoing electron line, are not shown.

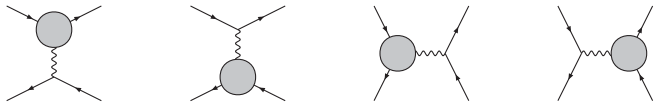

(a) (b) (c) (d)

FIG. 2. Two-loop photonic vertex diagrams contributing to Bhabha scattering.

$$F_1^{(2l,\mathrm{ph})}(t) = \frac{F_1^{(2l,\mathrm{ph},-2)}(t)}{(D-4)^2} + \frac{F_1^{(2l,\mathrm{ph},-1)}(t)}{(D-4)} + F_1^{(2l,\mathrm{ph},0)}(t) + \mathcal{O}(D-4),$$
$$F_2^{(2l,\mathrm{ph})}(t) = \frac{F_2^{(2l,\mathrm{ph},-1)}(t)}{(D-4)} + F_2^{(2l,\mathrm{ph},0)}(t) + \mathcal{O}(D-4), \quad (12)$$

where D is the dimensional regulator.

The four photonic two-loop vertex correction diagrams contributing to Bhabha scattering are shown in Fig. 2, where the shaded circle represents the sum of the vertex graphs shown[2] in Fig. 1.

The interference of diagrams 2(b) and 2(d) with the tree-level amplitude provides a contribution to the differential cross section that is identical to the one of diagrams 2(a) and 2(c), respectively. This can easily be proved by observing that diagram 2(b) [2(d)] can be obtained from 2(a) [2(c)] by applying the transformations $p_2 \leftrightarrow -p_3$ and $p_4 \leftrightarrow -p_1$ and that these transformations leave the Mandelstam invariants s and t unchanged.

The contribution of the diagram in Fig. 2(a) to the Bhabha scattering differential cross section at order α^4 can be written as

$$\left.\frac{d\sigma_2^{(V,\mathrm{ph\ Vertices})}}{d\Omega}\right|_{(\mathrm{ph\ Irr.Ver.,2a})} = \frac{\alpha^2}{s}\left[\frac{1}{st}V_1^{(2l,\mathrm{Irr.Ver.})}(s,t) + \frac{1}{t^2}V_2^{(2l,\mathrm{Irr.Ver.})}(s,t)\right]. \quad (13)$$

The functions $V_i^{(2l,\mathrm{Irr.Ver.})}(s,t)$ $(i=1,2)$ have the Laurent expansion

$$V_i^{(2l,\mathrm{Irr.Ver.})}(s,t) = \frac{V_i^{(2l,\mathrm{Irr.Ver.},-2)}(s,t)}{(D-4)^2} + \frac{V_i^{(2l,\mathrm{Irr.Ver.},-1)}(s,t)}{(D-4)} + V_i^{(2l,\mathrm{Irr.Ver.},0)}(s,t) + \mathcal{O}(D-4), \quad (14)$$

with

$$V_i^{(2l,\mathrm{Irr.Ver.},-2)}(s,t) = c_{i1}(s,t)\mathrm{Re}F_1^{(2l,\mathrm{ph},-2)}(t), \quad (15)$$

[2]The diagrams in Figs. 1(c) and 1(d) enter the sum with a multiplicity factor of 2.

$$V_i^{(2l,\mathrm{Irr.Ver.},-1)}(s,t) = c_{i1}(s,t)\mathrm{Re}F_1^{(2l,\mathrm{ph},-1)}(t) + c_{i2}(s,t)\mathrm{Re}F_1^{(2l,\mathrm{ph},-2)}(t) + c_{i3}(s,t)\mathrm{Re}F_2^{(2l,\mathrm{ph},-1)}(t), \quad (16)$$

$$V_i^{(2l,\mathrm{Irr.Ver.},0)}(s,t) = c_{i1}(s,t)\mathrm{Re}F_1^{(2l,\mathrm{ph},0)}(t) + c_{i2}(s,t)\mathrm{Re}F_1^{(2l,\mathrm{ph},-1)}(t) + c_{i4}(s,t)\mathrm{Re}F_1^{(2l,\mathrm{ph},-2)}(t) + c_{i3}(s,t)\mathrm{Re}F_2^{(2l,\mathrm{ph},0)}(t) + c_{i6}(s,t)\mathrm{Re}F_2^{(2l,\mathrm{ph},-1)}(t). \quad (17)$$

The functions c_{ij} are polynomials of the Mandelstam variables; their explicit expressions are collected in Appendix A, while the Laurent coefficients of the form factors $F_i^{(2l,\mathrm{ph})}$ $(i=1,2)$ were introduced in Eq. (12). Even if the form factors are real for a physical (spacelike) t, we write $\mathrm{Re}F_i^{(2l,\mathrm{ph})}(t)$ $(i=1,2)$ in the equations above for convenience of later use.

The contribution to the differential cross section of the interference of the diagram in Fig. 2(c) with the tree-level amplitude can be obtained from the contribution of diagram 2(a) by replacing $p_2 \leftrightarrow -p_3$. This is equivalent to exchanging $s \leftrightarrow t$, so that one finds

$$\left.\frac{d\sigma_2^{(V,\mathrm{ph\ Vertices})}}{d\Omega}\right|_{(\mathrm{ph\ Irr.Ver.,2c})} = \frac{\alpha^2}{s}\left[\frac{1}{s^2}V_2^{(2l,\mathrm{Irr.Ver.})}(t,s) + \frac{1}{st}V_1^{(2l,\mathrm{Irr.Ver.})}(t,s)\right]. \quad (18)$$

According to the definitions in Eqs. (15)–(17), the right-hand side of Eq. (18) involves the functions $F_i^{(2l,\mathrm{ph})}(s)$, which develop then an imaginary part above threshold ($s > 4m^2$). These imaginary parts do not contribute to the differential cross section at this order.

Finally, the total contribution of the four diagrams in Fig. 2 to the Bhabha scattering differential cross section at order α^4 is

$$\left.\frac{d\sigma_2^{(V,\mathrm{ph\ Vertices})}}{d\Omega}\right|_{(\mathrm{ph\ Irr.Ver.})} = 2\frac{\alpha^2}{s}\left[\frac{1}{s^2}V_2^{(2l,\mathrm{Irr.Ver.})}(t,s) + \frac{1}{t^2}V_2^{(2l,\mathrm{Irr.Ver.})}(s,t) + \frac{1}{st}(V_1^{(2l,\mathrm{Irr.Ver.})}(s,t) + V_1^{(2l,\mathrm{Irr.Ver.})}(t,s))\right]. \quad (19)$$

The first, second, and third terms within squared brackets in the right-hand side of Eq. (19) are the s-s, t-t, and s-t channel interference amplitudes, respectively.

IV. REDUCIBLE TWO-LOOP VERTEX CORRECTIONS

In this section, we consider the interference of the two-loop reducible vertex diagrams, shown in Fig. 3, with the tree-level Bhabha scattering amplitude. The two reducible diagrams contain a one-loop vertex correction in both fermionic currents. Their contribution to the differential cross section at order α^4 can be written in terms of the one-loop UV-renormalized vertex form factors $F_i^{(1l)}$ $(i = 1, 2)$ (see [12,26]) and of the functions c_{ij} $(i = 1, 2,\ j = 1, 6)$ introduced in the previous section. It must also be observed that the term linear in $(D - 4)$ is needed in the Laurent expansion of the one-loop vertex form factors.

The contribution of diagram 3(a) to the cross section is given by

$$\left.\frac{d\sigma_2^{(V,\text{ph Vertices})}}{d\Omega}\right|_{(\text{ph Red.Ver.,3a})} = \frac{\alpha^2}{s}\left[\frac{1}{st}V_1^{(2l,\text{Red.Ver.})}(s,t) + \frac{1}{t^2}V_2^{(2l,\text{Red.Ver.})}(s,t)\right], \tag{20}$$

where the Laurent expansion of $V_i^{(2l,\text{Red.Ver.})}$ is

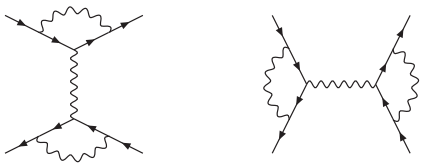

(a) (b)

FIG. 3. Two-loop reducible vertex diagrams contributing to Bhabha scattering.

$$V_i^{(2l,\text{Red.Ver.})} = \frac{V_i^{(2l,\text{Red.Ver.},-2)}}{(D-4)^2} + \frac{V_i^{(2l,\text{Red.Ver.},-1)}}{(D-4)} + V_i^{(2l,\text{Red.Ver.},0)} + \mathcal{O}(D-4), \tag{21}$$

with

$$V_i^{(2l,\text{Red.Ver.},-2)}(s,t) = c_{i1}(s,t)[(\text{Re}F_1^{(1l,-1)}(t))^2 - (\text{Im}F_1^{(1l,-1)}(t))^2], \tag{22}$$

$$V_i^{(2l,\text{Red.Ver.},-1)}(s,t) = c_{i2}(s,t)[(\text{Re}F_1^{(1l,-1)}(t))^2 - (\text{Im}F_1^{(1l,-1)}(t))^2] + 2c_{i1}(s,t)[\text{Re}F_1^{(1l,-1)}(t)\text{Re}F_1^{(1l,0)}(t) - \text{Im}F_1^{(1l,-1)}(t)\text{Im}F_1^{(1l,0)}(t)] + 2c_{i3}(s,t)[\text{Re}F_1^{(1l,-1)}(t)\text{Re}F_2^{(1l,0)}(t) - \text{Im}F_1^{(1l,-1)}(t)\text{Im}F_2^{(1l,0)}(t)], \tag{23}$$

$$\begin{aligned} V_i^{(2l,\text{Red.Ver.},0)}(s,t) = {} & c_{i4}(s,t)[(\text{Re}F_1^{(1l,-1)}(t))^2 - (\text{Im}F_1^{(1l,-1)}(t))^2] + 2c_{i2}(s,t)[\text{Re}F_1^{(1l,-1)}(t)\text{Re}F_1^{(1l,0)}(t) \\ & - \text{Im}F_1^{(1l,-1)}(t)\text{Im}F_1^{(1l,0)}(t)] + 2c_{i6}(s,t)[\text{Re}F_1^{(1l,-1)}(t)\text{Re}F_2^{(1l,0)}(t) - \text{Im}F_1^{(1l,-1)}(t)\text{Im}F_2^{(1l,0)}(t)] \\ & + 2c_{i1}(s,t)[\text{Re}F_1^{(1l,-1)}(t)\text{Re}F_1^{(1l,1)}(t) - \text{Im}F_1^{(1l,-1)}(t)\text{Im}F_1^{(1l,1)}(t)] + 2c_{i3}(s,t)[\text{Re}F_1^{(1l,-1)}(t)\text{Re}F_2^{(1l,1)}(t) \\ & - \text{Im}F_1^{(1l,-1)}(t)\text{Im}F_2^{(1l,1)}(t)] + c_{i1}(s,t)[(\text{Re}F_1^{(1l,0)}(t))^2 - (\text{Im}F_1^{(1l,0)}(t))^2] + 2c_{i3}(s,t) \\ & \times [\text{Re}F_1^{(1l,0)}(t)\text{Re}F_2^{(1l,0)}(t) - \text{Im}F_1^{(1l,0)}(t)\text{Im}F_2^{(1l,0)}(t)] + c_{i5}(s,t)[(\text{Re}F_2^{(1l,0)}(t))^2 - (\text{Im}F_2^{(1l,0)}(t))^2]. \end{aligned} \tag{24}$$

Similarly, the contribution of diagram 3(b) to the cross section at order α^4 is given by

$$\left.\frac{d\sigma_2^{(V,\text{ph Vertices})}}{d\Omega}\right|_{(\text{ph Red.Ver.,3b})} = \frac{\alpha^2}{s}\left[\frac{1}{st}V_1^{(2l,\text{Red.Ver.})}(t,s) + \frac{1}{s^2}V_2^{(2l,\text{Red.Ver.})}(t,s)\right]. \tag{25}$$

It is then possible to conclude that the interference of the diagrams in Fig. 3 with the tree-level amplitude gives the following contribution to the cross section:

$$\left.\frac{d\sigma_2^{(V,\text{ph Vertices})}}{d\Omega}\right|_{(\text{ph Red.Ver.})} = \frac{\alpha^2}{s}\left[\frac{1}{s^2}V_2^{(2l,\text{Red.Ver.})}(t,s) + \frac{1}{t^2}V_2^{(2l,\text{Red.Ver.})}(s,t) + \frac{1}{st}(V_1^{(2l,\text{Red.Ver.})}(s,t) + V_1^{(2l,\text{Red.Ver.})}(t,s))\right]. \tag{26}$$

The first, second, and third terms within squared brackets in the right-hand side of Eq. (26) are the s-s, t-t, and s-t channel interference amplitudes, respectively.

V. INTERFERENCE OF ONE-LOOP VERTEX DIAGRAMS

In this section, we obtain the Bhabha scattering cross section at order α^4 deriving from the interference of the diagrams in Fig. 4.

We begin by considering the contribution of the amplitude of diagram 4(a) squared; one finds that

$$\left.\frac{d\sigma_2^{(V,\text{ph Vertices})}}{d\Omega}\right|_{(\text{ph Ver.Ver.,4a})} = \frac{\alpha^2}{s}\frac{1}{t^2} I_1(s,t). \tag{27}$$

In Eq. (27), we introduce the function I_1 that has the following Laurent expansion in powers of $(D-4)$:

$$I_1(s,t) = \frac{I_1^{(-2)}(s,t)}{(D-4)^2} + \frac{I_1^{(-1)}(s,t)}{(D-4)} + I_1^{(0)}(s,t) + \mathcal{O}(D-4), \tag{28}$$

with

$$I_1^{(-2)}(s,t) = \tfrac{1}{2} c_{21}(s,t)[(\text{Re}F_1^{(1l,-1)}(t))^2 + (\text{Im}F_1^{(1l,-1)}(t))^2], \tag{29}$$

$$I_1^{(-1)}(s,t) = \tfrac{1}{2} c_{22}(s,t)[(\text{Re}F_1^{(1l,-1)}(t))^2 + (\text{Im}F_1^{(1l,-1)}(t))^2] + c_{21}(s,t)[\text{Re}F_1^{(1l,-1)}(t)\text{Re}F_1^{(1l,0)}(t) + \text{Im}F_1^{(1l,-1)}(t)\text{Im}F_1^{(1l,0)}(t)] + c_{23}(s,t)[\text{Re}F_1^{(1l,-1)}(t)\text{Re}F_2^{(1l,0)}(t) + \text{Im}F_1^{(1l,-1)}(t)\text{Im}F_2^{(1l,0)}(t)], \tag{30}$$

$$\begin{aligned} I_1^{(0)}(s,t) = {} & c_{22}(s,t)[\text{Re}F_1^{(1l,-1)}(t)\text{Re}F_1^{(1l,0)}(t) + \text{Im}F_1^{(1l,-1)}(t)\text{Im}F_1^{(1l,0)}(t)] + c_{21}(s,t)[\text{Re}F_1^{(1l,-1)}(t)\text{Re}F_1^{(1l,1)}(t) \\ & + \text{Im}F_1^{(1l,-1)}(t)\text{Im}F_1^{(1l,1)}(t)] + c_{22}(s,t)[\text{Re}F_1^{(1l,-1)}(t)\text{Re}F_2^{(1l,0)}(t) + \text{Im}F_1^{(1l,-1)}(t)\text{Im}F_2^{(1l,0)}(t)] \\ & + c_{23}(s,t)[\text{Re}F_1^{(1l,-1)}(t)\text{Re}F_2^{(1l,1)}(t) + \text{Im}F_1^{(1l,-1)}(t)\text{Im}F_2^{(1l,1)}(t)] + \tfrac{1}{2} c_{21}(s,t)[(\text{Re}F_1^{(1l,0)}(t))^2 + (\text{Im}F_1^{(1l,0)}(t))^2] \\ & + c_{23}(s,t)[\text{Re}F_1^{(1l,0)}(t)\text{Re}F_2^{(1l,0)}(t) + \text{Im}F_1^{(1l,0)}(t)\text{Im}F_2^{(1l,0)}(t)] + c_{27}(s,t)[(\text{Re}F_2^{(1l,0)}(t))^2 + (\text{Im}F_2^{(1l,0)}(t))^2]. \end{aligned} \tag{31}$$

The expression of the functions c_{ij} in terms of the Mandelstam invariants can be found in Appendix A, while the expression of the one-loop vertex form factors appearing in the functions I_1 can be found in Refs. [12,25] and are collected in Ref. [26].

Also, the contribution of the square of the diagram in Fig. 4(c) can be easily expressed by employing the function I_1:

$$\left.\frac{d\sigma_2^{(V,\text{ph Vertices})}}{d\Omega}\right|_{(\text{ph Ver.Ver.,4c})} = \frac{\alpha^2}{s}\frac{1}{s^2} I_1(t,s). \tag{32}$$

The interference between the diagrams in Figs. 4(a) and 4(b) generates a term in the cross section that can be written as

$$\left.\frac{d\sigma_2^{(V,\text{ph Vertices})}}{d\Omega}\right|_{(\text{ph Ver.Ver.,4a,b})} = \frac{\alpha^2}{s}\frac{1}{t^2} I_2(s,t), \tag{33}$$

where the function I_2 is given by

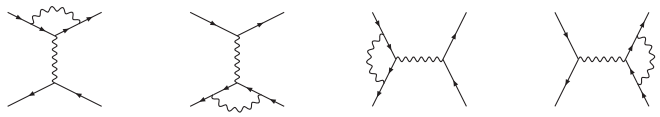

(a) (b) (c) (d)

FIG. 4. One-loop vertex diagrams contributing to Bhabha scattering.

$$I_2(s,t) = \frac{I_2^{(-2)}(s,t)}{(D-4)^2} + \frac{I_2^{(-1)}(s,t)}{(D-4)} + I_2^{(0)}(s,t) + \mathcal{O}(D-4), \tag{34}$$

with

$$I_2^{(-2)}(s,t) = 2I_1^{(-2)}(s,t), \tag{35}$$

$$I_2^{(-1)}(s,t) = 2I_1^{(-1)}(s,t), \tag{36}$$

$$\begin{aligned} I_2^{(0)}(s,t) = {} & 2I_1^{(0)}(s,t) + (c_{25}(s,t) - 2c_{27}(s,t)) \\ & \times [(\text{Re}F_2^{(1l,0)}(t))^2 + (\text{Im}F_2^{(1l,0)}(t))^2]. \end{aligned} \tag{37}$$

Similarly, the interference between the diagrams in Figs. 4(c) and 4(d) generates the following contribution to the differential cross section:

$$\left.\frac{d\sigma_2^{(V,\text{ph Vertices})}}{d\Omega}\right|_{(\text{ph Ver.Ver.,4c,d})} = \frac{\alpha^2}{s}\frac{1}{s^2} I_2(t,s). \tag{38}$$

The interference of the diagrams in Figs. 4(a) and 4(c) can be expressed in terms of a third function, I_3:

$$\left.\frac{d\sigma_2^{(V,\text{ph Vertices})}}{d\Omega}\right|_{(\text{ph Ver.Ver.,4a,c})} = \frac{\alpha^2}{s}\frac{1}{st} I_3(s,t). \tag{39}$$

Also in this case, it is convenient to explicitly write the Laurent expansion of the function I_3:

$$I_3(s,t) = \frac{I_3^{(-2)}(s,t)}{(D-4)^2} + \frac{I_3^{(-1)}(s,t)}{(D-4)} + I_3^{(0)}(s,t) + \mathcal{O}(D-4), \tag{40}$$

with

$$I_3^{(-2)}(s,t) = c_{11}(t,s) F_1^{(1l,-1)}(t) \mathrm{Re} F_1^{(1l,-1)}(s), \tag{41}$$

$$\begin{aligned} I_3^{(-1)}(s,t) = {} & c_{12}(t,s) F_1^{(1l,-1)}(t) \mathrm{Re} F_1^{(1l,-1)}(s) + c_{11}(t,s)[F_1^{(1l,-1)}(t) \mathrm{Re} F_1^{(1l,0)}(s) + F_1^{(1l,0)}(t) \mathrm{Re} F_1^{(1l,-1)}(s)] \\ & + c_{13}(t,s)[F_1^{(1l,-1)}(t) \mathrm{Re} F_2^{(1l,0)}(s) + F_2^{(1l,0)}(t) \mathrm{Re} F_1^{(1l,-1)}(s)], \end{aligned} \tag{42}$$

$$\begin{aligned} I_3^{(0)}(s,t) = {} & c_{14}(t,s) F_1^{(1l,-1)}(t) \mathrm{Re} F_1^{(1l,-1)}(s) + c_{12}(t,s)[F_1^{(1l,-1)}(t) \mathrm{Re} F_1^{(1l,0)}(s) + F_1^{(1l,0)}(t) \mathrm{Re} F_1^{(1l,-1)}(s)] + c_{11}(t,s) \\ & \times [F_1^{(1l,-1)}(t) \mathrm{Re} F_1^{(1l,1)}(s) + F_1^{(1l,1)}(t) \mathrm{Re} F_1^{(1l,-1)}(s)] + c_{16}(t,s) F_1^{(1l,-1)}(t) \mathrm{Re} F_2^{(1l,0)}(s) \\ & + c_{16}(s,t) F_2^{(1l,0)}(t) \mathrm{Re} F_1^{(1l,-1)}(s) + c_{13}(t,s) F_1^{(1l,-1)}(t) \mathrm{Re} F_2^{(1l,1)}(s) + c_{13}(s,t) F_2^{(1l,1)}(t) \mathrm{Re} F_1^{(1l,-1)}(s) \\ & + c_{13}(s,t) F_2^{(1l,0)}(t) \mathrm{Re} F_1^{(1l,0)}(s) + c_{13}(t,s) F_1^{(1l,0)}(t) \mathrm{Re} F_2^{(1l,0)}(s) + c_{17}(t,s) F_2^{(1l,0)}(t) \mathrm{Re} F_2^{(1l,0)}(s) \\ & + c_{11}(t,s) F_1^{(1l,0)}(t) \mathrm{Re} F_1^{(1l,0)}(s). \end{aligned} \tag{43}$$

Finally, it is easy to verify that all of the interferences between s- and t-channel diagrams in Fig. 4 give a contribution to the cross section identical to the one in Eq. (39), while the squared amplitude of the diagram 4(b) [4(d)] coincides with the squared amplitude of diagram 4(a) [4(c)]. We can then conclude that the total contribution of the interferences of the diagrams in Fig. 4 to the Bhabha scattering cross section is given by

$$\begin{aligned} \frac{d\sigma_2^{(V,\text{ph Vertices})}}{d\Omega}\bigg|_{(\text{ph Ver.Ver.})} = {} & \frac{\alpha^2}{s}\bigg[\frac{1}{t^2}(2I_1(s,t) + I_2(s,t)) \\ & + \frac{4}{st} I_3(s,t) + \frac{1}{s^2}(2I_1(t,s) \\ & + I_2(t,s))\bigg]. \end{aligned} \tag{44}$$

VI. INTERFERENCE OF ONE-LOOP VERTEX AND ONE-LOOP BOX DIAGRAMS

In the present section, we consider the interference of the diagrams in Fig. 4 with the diagrams in Fig. 5.

In order to write down the contributions that these interferences provide to the Bhabha scattering cross sections at order α^4, it is convenient to introduce the functions $I_{4,i}(x_1,x_2,x_3)$, where $i = 1,\ldots,3$ and where x_j ($j = 1,\ldots,3$) represents one of the Mandelstam invariants s, t, and u; these functions have the following Laurent expansion in $(D-4)$:

$$\begin{aligned} I_{4,i}(x_1,x_2,x_3) = {} & \frac{I_{4,i}^{(-2)}(x_1,x_2,x_3)}{(D-4)^2} + \frac{I_{4,i}^{(-1)}(x_1,x_2,x_3)}{(D-4)} \\ & + I_{4,i}^{(0)}(x_1,x_2,x_3) + \mathcal{O}(D-4). \end{aligned} \tag{45}$$

The coefficients of the Laurent expansion are given by

$$I_{4,i}^{(-2)}(x_1,x_2,x_3) = x_3 \mathrm{Re}[(F_1^{(1l,-1)}(x_1))^* B_i^{(1l,-1)}(x_2,x_3)], \tag{46}$$

$$\begin{aligned} I_{4,i}^{(-1)}(x_1,x_2,x_3) = {} & x_3 \mathrm{Re}[(F_1^{(1l,-1)}(x_1))^* B_i^{(1l,0)}(x_2,x_3) \\ & + (F_1^{(1l,0)}(x_1))^* B_i^{(1l,-1)}(x_2,x_3) \\ & + (F_2^{(1l,0)}(x_1))^* B_{i+3}^{(1l,-1)}(x_2,x_3)], \end{aligned} \tag{47}$$

$$\begin{aligned} I_{4,i}^{(0)}(x_1,x_2,x_3) = {} & x_3 \mathrm{Re}[(F_1^{(1l,-1)}(x_1))^* B_i^{(1l,1)}(x_2,x_3) \\ & + (F_1^{(1l,0)}(x_1))^* B_i^{(1l,0)}(x_2,x_3) \\ & + (F_1^{(1l,1)}(x_1))^* B_i^{(1l,-1)}(x_2,x_3) \\ & + (F_2^{(1l,0)}(x_1))^* B_{i+3}^{(1l,0)}(x_2,x_3) \\ & + (F_2^{(1l,1)}(x_1))^* B_{i+3}^{(1l,-1)}(x_2,x_3)]. \end{aligned} \tag{48}$$

Besides for the one-loop vertex form factors already employed in the previous sections, one encounters in the equations above the functions $B_i^{(1l,j)}$ ($i = 1,\ldots,3$, $j = -1, 0, 1$) introduced in Ref. [12] to describe the contribution of the diagrams in Fig. 5 to the Bhabha scattering cross

(a) (b) (c) (d)

FIG. 5. One-loop box diagrams contributing to Bhabha scattering.

section[3] at $\mathcal{O}(\alpha^3)$. The auxiliary functions $B_i^{(1l,j)}$ ($i = 4, \ldots, 6$, $j = -1, 0$) are introduced for the first time here, and their expressions in terms of HPLs and the dimensionless variables x, y, and z can be found in Ref. [26].

The interference of diagram 4(a) with diagram 5(a) gives the following contribution to the differential cross section:

$$\left.\frac{d\sigma_2^{(V,\text{ph Vertices})}}{d\Omega}\right|_{(\text{ph Ver.Box,4a,5a})} = \frac{\alpha^2}{4s}\frac{1}{t^2} I_{4,2}(t, s, t). \quad (49)$$

The notation has been chosen to clarify that Eq. (49) is related to the interference of two t-channel diagrams.

Similarly, it is possible to write all the interferences of diagrams 4(a) and 4(c) with the diagrams in Fig. 5 in terms of the functions $I_{4,i}$:

$$\left.\frac{d\sigma_2^{(V,\text{ph Vertices})}}{d\Omega}\right|_{(\text{ph Ver.Box,4a,5b})} = -\frac{\alpha^2}{4s}\frac{1}{t^2} I_{4,2}(t, u, t), \quad (50)$$

$$\left.\frac{d\sigma_2^{(V,\text{ph Vertices})}}{d\Omega}\right|_{(\text{ph Ver.Box,4a,5c})} = \frac{\alpha^2}{4s}\frac{1}{st} I_{4,1}(t, t, s), \quad (51)$$

$$\left.\frac{d\sigma_2^{(V,\text{ph Vertices})}}{d\Omega}\right|_{(\text{ph Ver.Box,4a,5d})} = \frac{\alpha^2}{4s}\frac{1}{st} I_{4,3}(t, u, s), \quad (52)$$

$$\left.\frac{d\sigma_2^{(V,\text{ph Vertices})}}{d\Omega}\right|_{(\text{ph Ver.Box,4c,5a})} = \frac{\alpha^2}{4s}\frac{1}{st} I_{4,1}(s, s, t), \quad (53)$$

$$\left.\frac{d\sigma_2^{(V,\text{ph Vertices})}}{d\Omega}\right|_{(\text{ph Ver.Box,4c,5b})} = \frac{\alpha^2}{4s}\frac{1}{st} I_{4,3}(s, u, t), \quad (54)$$

$$\left.\frac{d\sigma_2^{(V,\text{ph Vertices})}}{d\Omega}\right|_{(\text{ph Ver.Box,4c,5c})} = \frac{\alpha^2}{4s}\frac{1}{s^2} I_{4,2}(s, t, s), \quad (55)$$

$$\left.\frac{d\sigma_2^{(V,\text{ph Vertices})}}{d\Omega}\right|_{(\text{ph Ver.Box,4c,5d})} = -\frac{\alpha^2}{4s}\frac{1}{s^2} I_{4,2}(s, u, s). \quad (56)$$

The interference of diagram 4(b) [4(d)] with a diagram in Fig. 5 is identical to the interference of diagram 4(a) [4(c)] with the same diagram in Fig. 5. Therefore, the total contribution of the interferences between one-loop vertex diagrams and one-loop box diagrams to the Bhabha scattering cross section is twice the sum of Eqs. (49)–(56); namely,

$$\left.\frac{d\sigma_2^{(V,\text{ph Vertices})}}{d\Omega}\right|_{(\text{ph Ver.Box})} = \frac{\alpha^2}{2s}\left[\frac{1}{t^2}\left(I_{4,2}(t, s, t) - I_{4,2}(t, u, t)\right) - \frac{1}{st}\left(I_{4,1}(t, t, s) + I_{4,3}(t, u, s) + I_{4,1}(s, s, t) + I_{4,3}(s, u, t)\right) + \frac{1}{s^2}\left(I_{4,2}(s, t, s) - I_{4,2}(s, u, s)\right)\right]. \quad (57)$$

VII. INTERFERENCE OF ONE-LOOP BOX DIAGRAMS

With reference to Eq. (10), it is possible to further split $\sigma_2^{(V,\text{ph Boxes})}$ in the sum of two contributions; the first originates from the interference of two-loop photonic box diagrams and tree-level diagrams, the second originates from the interference of two one-loop box diagrams:

$$\frac{d\sigma_2^{(V,\text{ph Boxes})}}{d\Omega} = \left.\frac{d\sigma_2^{(V,\text{ph Boxes})}}{d\Omega}\right|_{(\text{ph BoxBox})} + \left.\frac{d\sigma_2^{(V,\text{ph Boxes})}}{d\Omega}\right|_{(\text{2LBox})}. \quad (58)$$

The two-loop photonic box diagrams in the $m \neq 0$ case are at the moment still unknown, and the calculation of the second term in the right-hand side of Eq. (58) currently remains as an open problem (see [20,21]).

On the contrary, the calculation of the first term in Eq. (58) is, in principle, straightforward. The interference of each pair of the one-loop box diagrams shown in Fig. 5 provides a contribution to the differential cross section of the form

$$\left.\frac{d\sigma_2^{(V,\text{ph Boxes})}}{d\Omega}\right|_{(\text{ph BoxBox},ij)} = \frac{\alpha^2}{4s} C_{ij}(x, y, z), \quad (59)$$

where the indices i, j run over the diagram labels ($i, j = a, b, c, d$) and where we have introduced new functions C_{ij}. The explicit expression of the latter, already continued to the physical region $s > 4m^2$, is particularly long and can be found in Ref. [26].

VIII. SOFT-PHOTON EMISSION AT ORDER α^4

All of the two-loop photonic corrections discussed in the previous sections are UV-renormalized, but they still include double and single poles in $(D - 4)$. These singular-

[3]While the analytic expressions of the functions $B_i^{(1l,-1)}$ and $B_i^{(1l,0)}$ are explicitly given in Ref. [12], the expressions of the functions $B_i^{(1l,1)}$ are not. They are the coefficients of $(D - 4)$ in the Laurent expansion of the functions $B_i^{(1l)}$ [Eq. (45) in Ref. [12]] that were not needed in that context. Their expression in terms of HPLs and dimensionless variables can be found in Ref. [26].

ities have an IR origin, and they can be eliminated by adding the contribution of the real soft-photon emission diagrams at order α^4 to the virtual cross section.

Before discussing the soft corrections to the Bhabha scattering differential cross section of order α^4, the reader is reminded that the soft corrections at order α^3, discussed in detail in Ref. [13], can be written in the factorized form

$$\left(\frac{\alpha}{\pi}\right)\frac{d\sigma_1^S(s,t,m^2)}{d\Omega} = \left(\frac{\alpha}{\pi}\right)\frac{d\sigma_0^D(s,t,m^2)}{d\Omega} S_{\rm IR}, \qquad (60)$$

where $\sigma_0^D(s,t,m^2)$ is the tree-level cross section obtained by calculating the traces of Dirac matrices in D dimensions and where $S_{\rm IR}$ is defined as

$$S_{\rm IR} \equiv 4\sum_{j=1}^{4} J_{1j}, \qquad J_{1j} = \epsilon_j (p_1 \cdot p_j) I_{1j}, \qquad (61)$$

with $\epsilon_1 = \epsilon_4 = 1$ and $\epsilon_2 = \epsilon_3 = -1$, and

$$I_{1j} = \frac{1}{\Gamma(3-\frac{D}{2})\pi^{(D-4)/2}} \frac{m^{(D-4)}}{4\pi^2} \int^{\omega} \frac{d^{D-1}k}{k_0} \times \frac{1}{(p_1\cdot k)(p_j \cdot k)}. \qquad (62)$$

The integral in Eq. (62) can be found in Ref. [27] (see also Appendix A of Ref. [13]); the integration over the momentum of the soft photon (k) is restricted to the region $|\vec{k}| = k_0 < \omega$, where ω is the cutoff on the energy of the unobserved soft photon. The expansion of $\sigma_0^D(s,t,m^2)$ in powers of $(D-4)$ is

$$\frac{d\sigma_0^D(s,t,m^2)}{d\Omega} = \frac{d\sigma_0(s,t,m^2)}{d\Omega} + (D-4)\frac{d\sigma_0^{(1)}(s,t,m^2)}{d\Omega} + (D-4)^2 \frac{d\sigma_0^{(2)}(s,t,m^2)}{d\Omega} + \mathcal{O}((D-4)^3), \qquad (63)$$

where $\sigma_0(s,t,m^2)$ is the well known tree-level cross section, and

$$\frac{d\sigma_0^{(1)}(s,t,m^2)}{d\Omega} = \frac{\alpha^2}{s}\left\{\frac{1}{s^2}\left[\frac{s^2}{4}\right] + \frac{1}{t^2}\left[\frac{t^2}{4}\right] + \frac{1}{st}\left[\frac{1}{2}(s+t)^2 - \frac{1}{2}st - m^2(s+t)\right]\right\}, \qquad (64)$$

$$\frac{d\sigma_0^{(2)}(s,t,m^2)}{d\Omega} = \frac{\alpha^2}{s}\frac{1}{st}\left[-\frac{1}{4}st\right]. \qquad (65)$$

The contribution of the s- and t- channel diagrams, and of their interference to $\sigma_0^{(1)}(s,t,m^2)$ and $\sigma_0^{(2)}(s,t,m^2)$, is evident in Eqs. (64) and (65).

There are two different kinds of soft-photon emission diagrams contributing to the real corrections to the cross section at order α^4:

(i) the tree-level diagrams with the emission of two soft photons [some diagrams belonging to this class are shown in Figs. 6(a)–6(d)] and
(ii) the diagrams which include a one-loop correction and the emission of a soft photon from one of the external legs [see the examples in Fig. 6(e)–6(h)].

Since the soft-photon corrections in QED exponentiate, the contribution of the double emission diagrams to the Bhabha scattering differential cross section is given by

$$\left(\frac{\alpha}{\pi}\right)^2 \frac{d\sigma_2^{(S,\rm double)}(s,t,m^2)}{d\Omega} = \frac{1}{2}\left(\frac{\alpha}{\pi}\right)^2 \frac{d\sigma_0^D(s,t,m^2)}{d\Omega}(S_{\rm IR})^2. \qquad (66)$$

The emission of a single photon from one-loop diagrams, interfered with the tree-level single-photon emission graphs, amounts to

$$\left(\frac{\alpha}{\pi}\right)^2 \frac{d\sigma_2^{(S,\rm single)}(s,t,m^2)}{d\Omega} = \left(\frac{\alpha}{\pi}\right)^2 \frac{d\sigma_1^{(V,D)}(s,t,m^2)}{d\Omega} S_{\rm IR}, \qquad (67)$$

where $\sigma_1^{(V,D)}$ is the UV-renormalized virtual cross section at order α^3. The superscript D was introduced as a reminder that the Laurent expansion of $\sigma_1^{(V,D)}$ must be known up to and including terms linear in $(D-4)$; the reason for this is that these linear terms give rise to a finite contribution when multiplied by the single pole present in $S_{\rm IR}$. The real corrections of order α^4 which originate from single-photon emission diagrams and which include a fermionic loop [as, for example, diagram 6(h)], were calculated in Ref. [13]; they include single IR poles that cancel against the virtual corrections of order α^4 that also include a photon self-energy insertion. This set does not play any role to the present discussion and is thus systematically ignored.

With the above in mind, the one-loop virtual cross section appearing in Eq. (67) can be written as

$$\frac{d\sigma_1^{(V,D)}(s,t,m^2)}{d\Omega} = \left.\frac{d\sigma_1^{(V,D)}(s,t,m^2)}{d\Omega}\right|_{(1l,V)} + \left.\frac{d\sigma_1^{(V,D)}(s,t,m^2)}{d\Omega}\right|_{(1l,B)}, \qquad (68)$$

where the subscript V indicates the contribution of the interference between vertex graphs and tree-level amplitude; B stands for the cross section generated by the interference between one-loop boxes and tree-level diagrams. Furthermore, we split the terms on the right-hand side of Eq. (68) as follows:

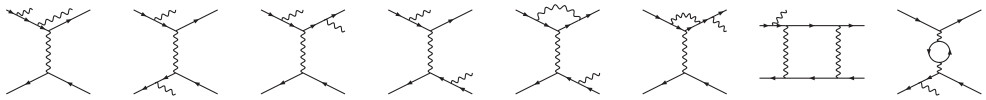

FIG. 6. Examples of double-photon emission from tree-level diagrams and single-photon emission from one-loop diagrams.

$$\left.\frac{d\sigma_1^{(V,D)}(s,t,m^2)}{d\Omega}\right|_{(1l,j)} = \left.\frac{d\sigma_1^{V}(s,t,m^2)}{d\Omega}\right|_{(1l,j)} + (D-4)\left.\frac{d\sigma_1^{(V,1)}(s,t,m^2)}{d\Omega}\right|_{(1l,j)} + \mathcal{O}((D-4)^2), \tag{69}$$

with $j = V, B$. The singular and finite parts of the one-loop virtual cross section, corresponding to the first term in the right-hand side of Eq. (68), are well known. Their expression in terms of Mandelstam invariants and HPLs can be found in Eqs. (43) and (49) of Ref. [12]. The terms proportional to $(D-4)$ which arise from box and vertex one-loop corrections are given by

$$\left.\frac{d\sigma_1^{(V,1)}(s,t,m^2)}{d\Omega}\right|_{(1l,B)} = \frac{\alpha^2}{s}\left[\frac{m^2}{s}(\mathrm{Re}B_1^{(1l,1)}(s,t) + \mathrm{Re}B_2^{(1l,1)}(t,s) + B_3^{(1l,1)}(u,t) - \mathrm{Re}B_2^{(1l,1)}(u,s)) + \frac{m^2}{t}(\mathrm{Re}B_2^{(1l,1)}(s,t) + \mathrm{Re}B_1^{(1l,1)}(t,s) - B_2^{(1l,1)}(u,t) + \mathrm{Re}B_3^{(1l,1)}(u,s))\right] \tag{70}$$

and

$$\left.\frac{d\sigma_1^{(V,1)}(s,t,m^2)}{d\Omega}\right|_{(1l,V)} = 2\frac{\alpha^2}{s}\left[\frac{1}{s^2}V_2^{(1l,1)}(t,s) + \frac{1}{t^2}V_2^{(1l,1)}(s,t) + \frac{1}{st}(V_1^{(1l,1)}(t,s) + V_1^{(1l,1)}(s,t))\right], \tag{71}$$

respectively, with

$$V_i^{(1l,1)}(s,t) = c_{i1}(s,t)\mathrm{Re}F_1^{(1l,1)}(t) + c_{i2}(s,t)\mathrm{Re}F_1^{(1l,0)}(t) + c_{i4}(s,t)\mathrm{Re}F_1^{(1l,-1)}(t) + c_{i6}(s,t)\mathrm{Re}F_2^{(1l,0)}(t) + c_{i3}(s,t)\mathrm{Re}F_2^{(1l,1)}(t), \qquad (i = 1, 2). \tag{72}$$

All of the functions appearing in the right-hand side of Eqs. (70)–(72) were introduced in the previous sections, and their expressions in terms of Mandelstam invariants and HPLs have been collected in Ref. [26].

As is mentioned above, the calculation of the integrals I_{1j} which appears in Eq. (61) has been carried out in Ref. [13], up to terms linear in $(D-4)$ excluded. At first glance, it appears that the calculation of such terms is needed, since they provide, in the limit $D \to 4$, a nonvanishing contribution to both Eqs. (66) and (67). However, it is possible to prove that this is not the case. In order to proceed with our proof, one needs to split the one-loop UV-renormalized virtual corrections in an IR-divergent part and a finite reminder, as is exemplified in the following:

$$\left.\frac{d\sigma_1^{V}(s,t,m^2)}{d\Omega}\right|_{(1l,j)} = \frac{1}{(D-4)}\left.\frac{d\sigma_1^{(V,-1)}(s,t,m^2)}{d\Omega}\right|_{(1l,j)} + \left.\frac{d\sigma_1^{(V,0)}(s,t,m^2)}{d\Omega}\right|_{(1l,j)}. \tag{73}$$

The Laurent expansion of S_{IR} has the form

$$S_{\mathrm{IR}} = \frac{S_{\mathrm{IR}}^{(-1)}}{(D-4)} + S_{\mathrm{IR}}^{(0)} + (D-4)S_{\mathrm{IR}}^{(1)} + \mathcal{O}((D-4)^2). \tag{74}$$

The cancellation of IR divergencies in the order α^3 cross section guarantees that[4]

$$\left.\frac{d\sigma_1^{(V,-1)}(s,t,m^2)}{d\Omega}\right|_{(1l,B)} + \left.\frac{d\sigma_1^{(V,-1)}(s,t,m^2)}{d\Omega}\right|_{(1l,V)} + \frac{d\sigma_0(s,t,m^2)}{d\Omega}S_{\mathrm{IR}}^{(-1)} = 0. \tag{75}$$

By employing Eqs. (66) and (67) in combination with Eqs. (63), (73), and (74), one can prove that the nonvanishing term proportional to $S_{\mathrm{IR}}^{(1)}$ appearing in the double emission cross section [Eq. (66)] is

[4]We remind the reader that the photon self-energy diagrams are IR-finite (see [13]).

$$\frac{d\sigma_2^{(S,\mathrm{double})}(s,t,m^2)}{d\Omega} \to \frac{d\sigma_0(s,t,m^2)}{d\Omega} S_{\mathrm{IR}}^{(-1)} S_{\mathrm{IR}}^{(1)}, \qquad (76)$$

while the nonvanishing term proportional to $S_{\mathrm{IR}}^{(1)}$ appearing in the single-photon emission cross sections at order α^4 is

$$\frac{d\sigma_2^{(S,\mathrm{single})}(s,t,m^2)}{d\Omega} \to \left[\frac{d\sigma_1^{(V,-1)}(s,t,m^2)}{d\Omega}\bigg|_{(1l,B)} + \frac{d\sigma_1^{(V,-1)}(s,t,m^2)}{d\Omega}\bigg|_{(1l,V)} \right] S_{\mathrm{IR}}^{(1)}. \qquad (77)$$

Therefore, we can conclude that, due to Eq. (75), the nonvanishing terms proportional to $S_{\mathrm{IR}}^{(1)}$ cancel out in the total real emission cross section at order α^4, given by the sum of Eqs. (66) and (67).

IX. CANCELLATION OF THE IR SINGULARITIES

The IR divergencies in the real corrections at order α^4 [Eqs. (66) and (67)] should cancel the IR singularities present in the virtual corrections discussed in Secs. III, IV, V, VI, and VII and the ones arising from the interference of the (yet unknown) two-loop photonic box graphs with the tree-level amplitude.

As in the case of the cancellation of the IR divergencies of the virtual cross section at order $\alpha^4(N_F = 1)$ discussed in Ref. [13], it is possible to organize the contributions to the cross section in IR-finite blocks by pairing the virtual corrections originating from a certain set of diagrams with an appropriate subset of the soft-photon emission corrections. As an example, in the first line in Fig. 7 we illustrate the cancellation of the IR poles present in the interference of the graph in Fig. 2(a) with the t-channel tree-level diagram; in all the terms in the left-hand side, the product of two graphs represents the contribution of their interference to the Bhabha scattering differential cross section. Once again, the gray circle represents the sum of the UV-renormalized two-loop photonic vertex corrections to the electron current in the t-channel photon-exchange diagram. In the second line in Fig. 7, we provide another example of the cancellation of the IR divergencies in the box-by-box sector. Similar relations can be found for all of the contributions to the cross section at order α^4.

A special case is represented by the virtual corrections in which the coefficients of the IR poles, when calculated in the nonphysical region $s < 0$, include HPLs with two or more zeros in the rightmost positions in the weight list.

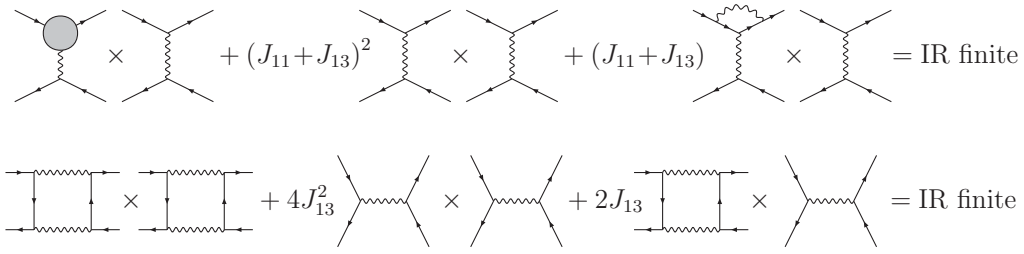

FIG. 7. Example of the cancellation of the IR divergencies in the two-loop irreducible vertex corrections (first line) and in the interference of the one-loop direct box in the s channel with itself (second line).

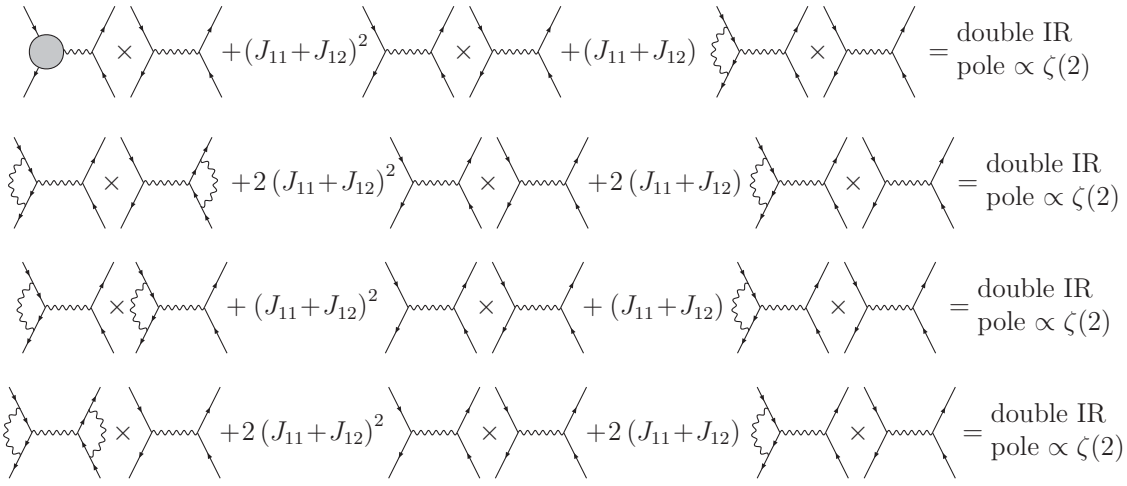

FIG. 8. Residual IR poles proportional to $\zeta(2)$ in the s-channel cross section.

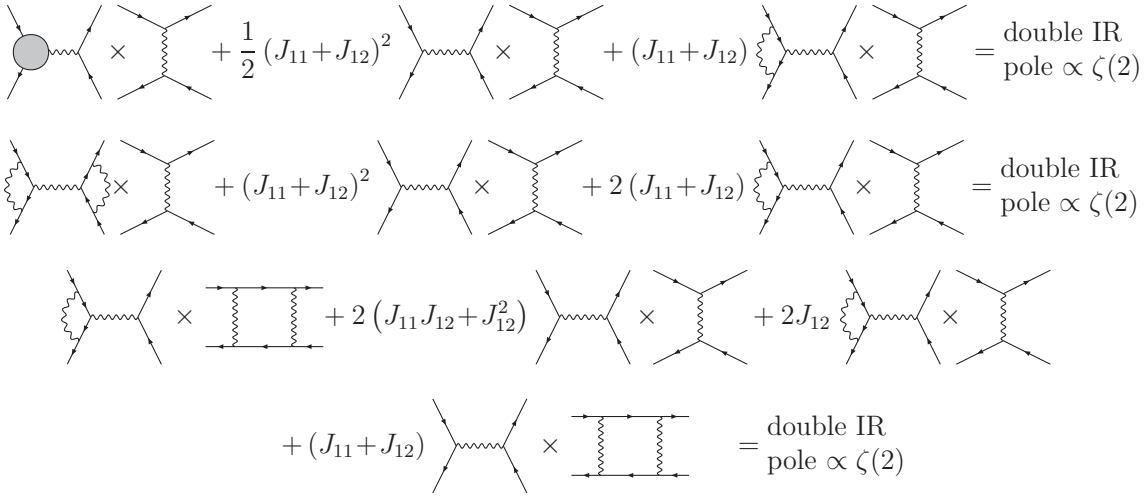

FIG. 9. Residual IR poles proportional to $\zeta(2)$ in the s-t-channel interference contribution to $\sigma_2^{(V,\text{ph Vertices})}$.

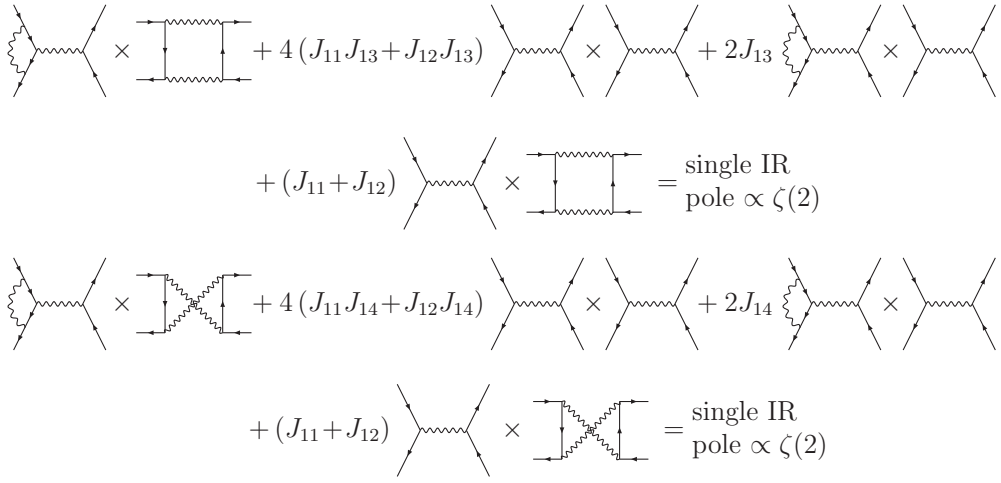

FIG. 10. Residual IR single poles proportional to $\zeta(2)$ in the interference of one-loop vertex by one-loop box diagrams.

When performing the analytic continuation to the physical region $s > 4m^2$, these HPLs generate real terms proportional to $\zeta(2)$, where ζ is the Riemann Zeta function. For example, by replacing the nonphysical dimensionless variable x according to $x \to -x' + i\epsilon$, one finds that

$$H(0,0;x) \to H(0,0;-x'+i\epsilon) = H(0,0;x') - 3\zeta(2) + i\pi H(0;x') \tag{78}$$

or

$$H(-1,0,0;x) \to H(-1,0,0;-x'+i\epsilon) = -H(1,0,0;x') + 3\zeta(2) - i\pi H(1,0;x'). \tag{79}$$

The part of the IR pole which is proportional to the $\zeta(2)$ factor arising from analytic continuation does not cancel in the combination with the soft-radiation contributions that eliminate the other IR singularities. This kind of behavior, already observed in Ref. [13] in the discussion of the $\mathcal{O}(\alpha^4(N_F = 1))$ cross section, is again encountered in the cases illustrated in Figs. 8–11.

In the total differential cross section, the residual poles of Fig. 8 cancel themselves out. Combining the various contributions shown in Fig. 9, the residual IR poles do not cancel. Residual single poles proportional to $\zeta(2)$ also arise in the combinations shown in Figs. 10 and 11. Clearly, such residual poles cancel once the contribution of the two-loop box graphs is included in the cross section at order α^4. The five two-loop photonic box topologies are shown in Fig. 12.

X. LOGARITHMIC EXPANSIONS

In order to check our calculations against the results available in the literature, the contributions to the cross section at order α^4 described in the previous sections are expanded in the limit in which the mass of the electron is small with respect to all of the Mandelstam

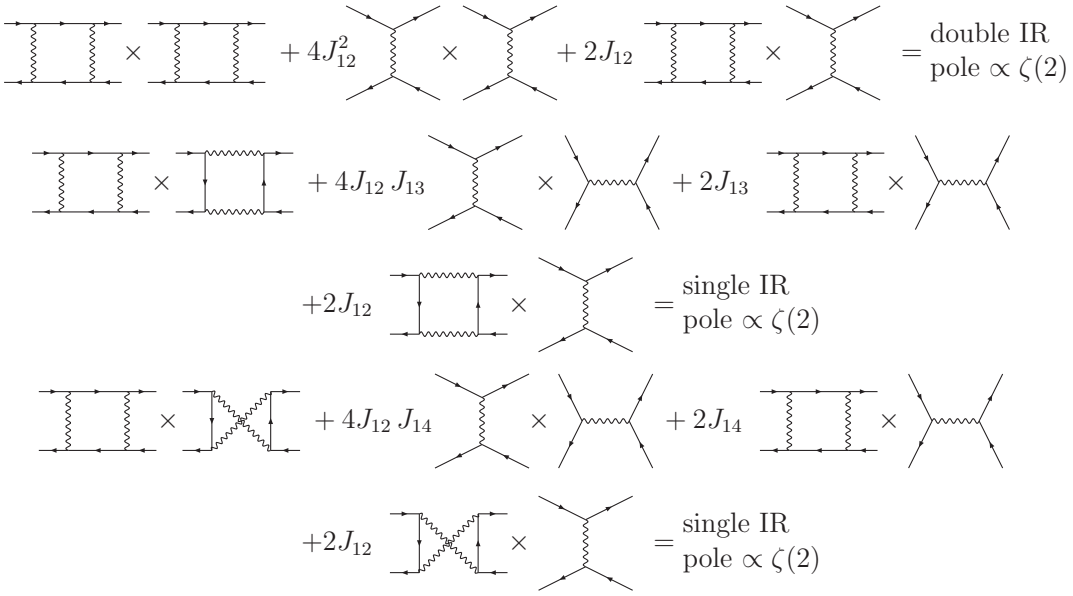

FIG. 11. Residual IR poles proportional to $\zeta(2)$ in the interference amongst one-loop box diagrams.

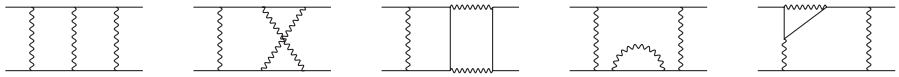

FIG. 12. Two-loop photonic box topologies.

invariants[5] s, t, and u. In this limit, it is customary to write the two-loop photonic cross section as follows (see [6,10]):

$$\frac{d\sigma_2^{(\mathrm{ph})}}{d\sigma_0} \equiv \sum_i \frac{d\sigma_2^{(V,i)} + d\sigma_2^{(S,i)}}{d\sigma_0} = \delta_2^{(2)} \ln^2\left(\frac{s}{m^2}\right) + \delta_2^{(1)} \ln\left(\frac{s}{m^2}\right) + \delta_2^{(0)} + \mathcal{O}\left(\frac{m^2}{s}\right). \quad (80)$$

In the equation above, $i = \mathrm{ph\ Vertices}, \mathrm{ph\ Boxes}$. Following the notation adopted in the previous sections,

$$\frac{d\sigma_2^{(V,\mathrm{ph\ Vertices})}}{d\Omega} = \left.\frac{d\sigma_2^{(V,\mathrm{ph\ Vertices})}}{d\Omega}\right|_{(\mathrm{ph\ Irr.Ver.})} + \left.\frac{d\sigma_2^{(V,\mathrm{ph\ Vertices})}}{d\Omega}\right|_{(\mathrm{ph\ Red.Ver.})} + \left.\frac{d\sigma_2^{(V,\mathrm{ph\ Vertices})}}{d\Omega}\right|_{(\mathrm{ph\ Ver.Ver.})} + \left.\frac{d\sigma_2^{(V,\mathrm{ph\ Vertices})}}{d\Omega}\right|_{(\mathrm{ph\ Ver.Box})}, \quad (81)$$

[5]Note that this expansion is not valid for very small scattering angles, corresponding to $|t| < m^2$, and for almost-backward scattering, corresponding to $|u| < m^2$.

while $\sigma_2^{(V,\mathrm{ph\ Boxes})}$ was introduced in Sec. VII. The corresponding $\sigma_2^{(S,i)}$ cross sections were obtained by pairing virtual and soft-photon emission contributions as described in Sec. IX. In several points of our discussion, we stressed the fact that a nonapproximated calculation of the contribution of the two-loop photonic box diagrams to the cross section is still missing. However, all of the coefficients $\delta_2^{(i)}$ $(i = 2, 1, 0)$ in the expansion in Eq. (80) are completely known; the first two can be found in Ref. [6], while $\delta_2^{(0)}$ was recently obtained in Ref. [10]. Therefore, by employing the $m^2/s \to 0$ limit of the results presented here in combination with Refs. [6,10], it is possible to indirectly obtain the $m^2/s \to 0$ limit of the contribution of the yet unknown two-loop photonic boxes (and corresponding soft-photon emission corrections). In Appendix B, we report the expression of such a contribution, both before and after adding the corresponding soft-photon corrections. Moreover, the expansions in the $m^2/s \to 0$ limit of all the contributions to the Bhabha scattering cross section discussed in the present paper can be found in Ref. [26].

It is known that the small-angle Bhabha scattering cross section is completely determined by the Dirac vertex form factor [4]. In particular, one finds that for the virtual cross section

$$\frac{d\sigma_2^{(V,\mathrm{ph})}}{d\sigma_0} \overset{\theta\to 0}{=} 6(F_1^{(1l)}(t))^2 + 4F_1^{(2l,\mathrm{ph})}(t), \tag{82}$$

where $F_1^{(1l)}$ and $F_1^{(2l,\mathrm{ph})}$ are the UV-renormalized vertex form factors already employed in this paper. The IR poles present in the form factors are easily removed by adding the soft emission contributions. By introducing the IR-finite form factors

$$\begin{aligned}\tilde{F}_1^{(1l)}(t) &= F_1^{(1l)}(t) + J_{11} + J_{13},\\ \tilde{F}_1^{(2l,\mathrm{ph})}(t) &= F_1^{(2l,\mathrm{ph})}(t) + \tfrac{1}{2}(J_{11} + J_{13})^2,\end{aligned} \tag{83}$$

where J_{1j} are defined in Eq. (61), one finds that

$$\begin{aligned}\frac{d\sigma_2^{(\mathrm{ph})}}{d\sigma_0} &\overset{\theta\to 0}{=} 6(\tilde{F}_1^{(1l)}(t))^2 + 4\tilde{F}_1^{(2l,\mathrm{ph})}(t)\\ &= \frac{1}{(1-\xi+\xi^2)^2}\left\{\ln^2\left(\frac{s}{m^2}\right)\left[\frac{9}{2} + 2\ln^2\left(\frac{4\omega^2}{s}\right) + 6\ln\left(\frac{4\omega^2}{s}\right)\right]\right.\\ &\quad + \ln\left(\frac{s}{m^2}\right)\left[6\zeta(3) - 3\zeta(2) - \frac{93}{8} + 9\ln(\xi) - 4\ln^2\left(\frac{4\omega^2}{s}\right)[1-\ln(\xi)] - 2\ln\left(\frac{4\omega^2}{s}\right)[7-6\ln(\xi)]\right]\\ &\quad - 9\zeta(3) + \frac{51}{4}\zeta(2) - 12\zeta(2)\ln(2) - \frac{32}{5}\zeta^2(2) + \frac{27}{2} + 6\zeta(3)\ln(\xi) - 3\zeta(2)\ln(\xi) - \frac{93}{8}\ln(\xi) + \frac{9}{2}\ln(\xi)^2\\ &\quad \left. + \ln^2\left(\frac{4\omega^2}{s}\right)[2 - 4\ln(\xi) + 2\ln^2(\xi)] + \ln\left(\frac{4\omega^2}{s}\right)[8 - 14\ln(\xi) + 6\ln^2(\xi)] + \mathcal{O}(\xi)\right\}.\end{aligned} \tag{84}$$

The variable ξ is defined as

$$\xi = \frac{1-\cos\theta}{2}, \tag{85}$$

with θ the scattering angle in the c.m. frame. By expanding the exact photonic corrections involving vertex diagrams in the $\theta \to 0$ limit and by neglecting terms proportional to the electron mass, we recover the expression in Eq. (84), which agrees with Ref. [10] and the theorem in Ref. [4]. Consequently, this represents a nontrivial test of our calculation. As expected, we observe that the interference between one-loop box diagrams and one-loop vertex corrections does not contribute to the small-angle cross section. The interference of one-loop box diagrams amongst themselves has a nonzero small-angle limit, and all of the residual terms are proportional to $\zeta(2)$. These residual terms cancel out once the contribution of the two-loop photonic boxes is added; for this reason they are excluded from the present discussion. The agreement with the results of Ref. [10] is clarified in Fig. 13, where we plot as a function of the scattering angle θ the result of Ref. [10] and the corrections of order α^4 originating from vertex graphs (Secs. III, IV, V, and VI, plus corresponding soft emission contributions). It is easily seen that, at small angles, the vertex corrections completely determine the cross section.

In addition, the expansion of the interference of one-loop boxes provides another strong test of both our calculation and the one discussed in Ref. [10]. The interference of some pairs of the diagrams in Fig. 5 gives origin, in the ratio $d\sigma_2/d\sigma_0$, to terms proportional to

$$\frac{\ln^n\xi}{(1-\xi)^m}, \qquad n = 1,\cdots,4; \qquad m = 1,2. \tag{86}$$

It is possible to observe that, in the sum of all the one-loop box interferences, such terms cancel out and that they do not appear in the complete photonic cross section at order α^4 [10].

The photonic corrections to the Bhabha scattering cross section are now known up to terms of $\mathcal{O}(m^2/s)$ excluded; it is possible to use the corrections calculated exactly in this work to estimate the relevance of the $\mathcal{O}(m^2/s)$ terms. We define

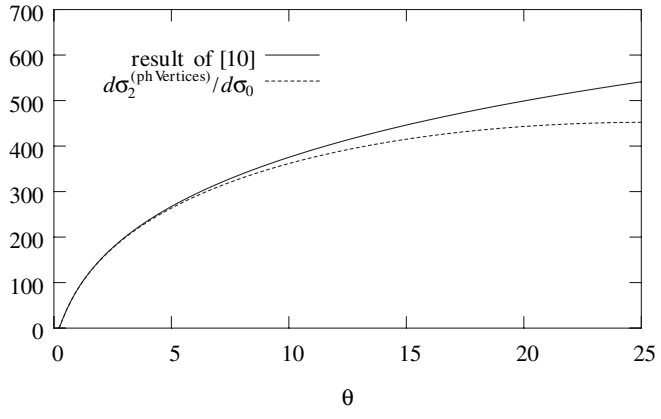

FIG. 13. Order α^4 Bhabha scattering differential cross section divided by the cross section in Born approximation, as a function of the scattering angle θ. The continuous line represents the result of Ref. [10], while the dashed line represents the corrections involving at least a vertex graph. The beam energy is chosen equal to 0.5 GeV, and the soft-photon energy cutoff ω is set equal to E.

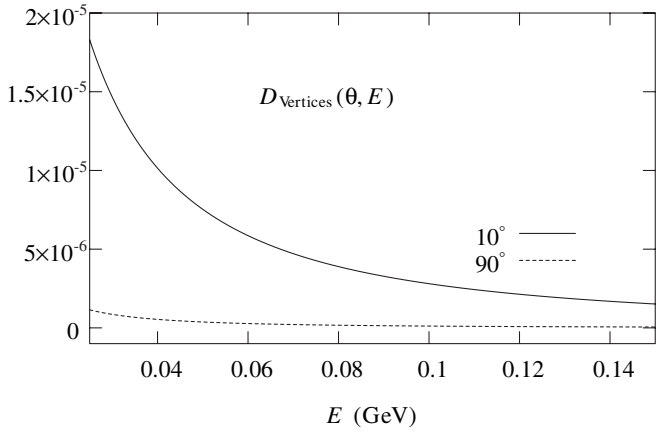

FIG. 14. $D_{\rm Vertices}$ as a function of the beam energy, for $\theta = 10°$ (solid line) and $\theta = 90°$ (dashed line). The soft-photon energy cutoff is set equal to E.

$$\frac{d\sigma_2^{(\mathrm{ph}\ i)}}{d\Omega} = \frac{d\sigma_2^{(V,i)} + d\sigma_2^{(S,i)}}{d\Omega} = \frac{d\sigma_2^{(\mathrm{ph}\ i)}}{d\Omega}\bigg|_L + \mathcal{O}\left(\frac{m^2}{s}, \frac{m^2}{t}, \frac{m^2}{u}\right), \tag{87}$$

where the index $i =$ Vertices, BoxBox represents the contributions discussed in Secs. III, IV, V, and VI, and VII, respectively. In Figs. 14 and 15, we plot, as a function of the beam energy, the quantities

$$D_i = \left(\frac{\alpha}{\pi}\right)^2 \left| \left(\frac{d\sigma_2^{(\mathrm{ph}\ i)}}{d\Omega} - \frac{d\sigma_2^{(\mathrm{ph}\ i)}}{d\Omega}\bigg|_L \right) \right| \times \left(\frac{d\sigma_0}{d\Omega} + \left(\frac{\alpha}{\pi}\right) \frac{d\sigma_1}{d\Omega} \right)^{-1}. \tag{88}$$

It can be seen from these plots that the terms proportional to the electron mass become negligible for values of the beam energy that are very small with respect to the ones encountered in practically all of the e^+e^- experiments. It is also reasonable to expect that the terms proportional to the electron mass are negligible in the corrections due to the two-loop photonic boxes. In this sense, the approximated cross section obtained in Refs. [6,10,12,13] should be sufficient for all phenomenological studies.

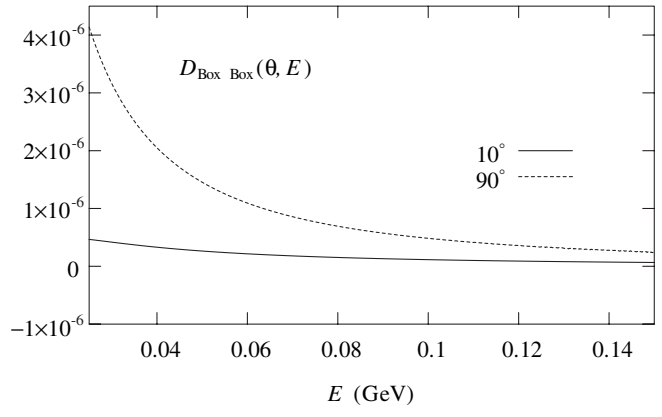

FIG. 15. $D_{\rm BoxBox}$ as a function of the energy, for $\theta = 10°$ (solid line) and $\theta = 90°$ (dashed line). The soft-photon energy cutoff is set equal to E.

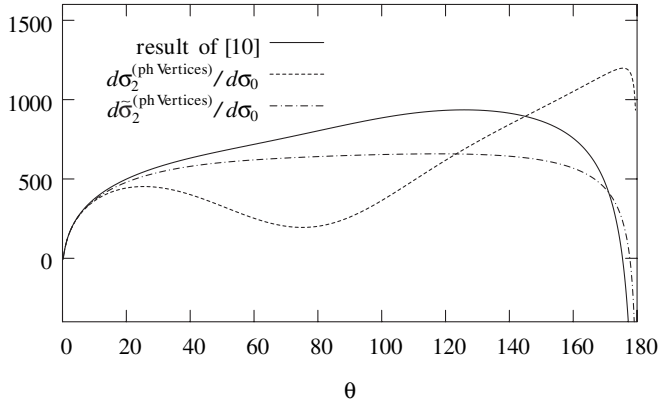

FIG. 16. Comparison of the vertex corrections with the complete photonic cross section at order α^4. E and ω as in Fig. 13.

Finally, in Figs. 16 and 17, it is possible to compare the various contributions to the Bhabha scattering differential cross section known at present with the complete photonic cross section in the $m^2/s \to 0$ limit [10]. The dashed line in Fig. 16 corresponds to the contribution to the cross section defined in Eq. (87) for $i =$ Vertices, plotted as a function of the scattering angle. The local minimum at $\theta \sim 80°$ and the maximum in the backward direction are due to spurious terms proportional to the monomials

$$\zeta(2)\ln^2\left(\frac{s}{m^2}\right), \qquad \zeta(2)\ln\left(\frac{s}{m^2}\right)\ln\xi, \qquad \text{and} \qquad \zeta(2)\ln\left(\frac{s}{m^2}\right)\ln(1-\xi). \tag{89}$$

These terms are not present in the complete cross section (they cancel out against analogous contributions deriving from the interferences of two-loop box diagrams with the

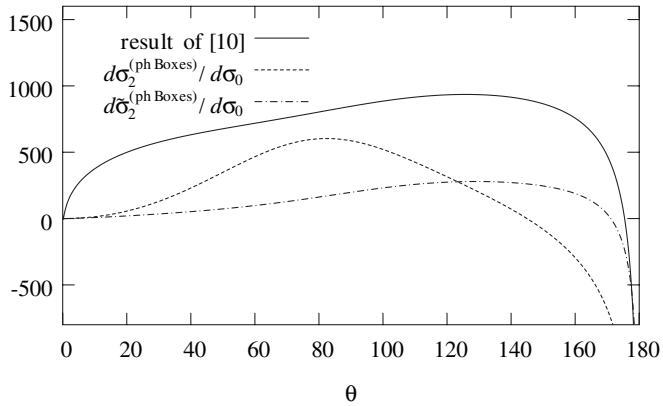

FIG. 17. Comparison of the box corrections with the complete photonic cross section at order α^4. E and ω as in Fig. 13.

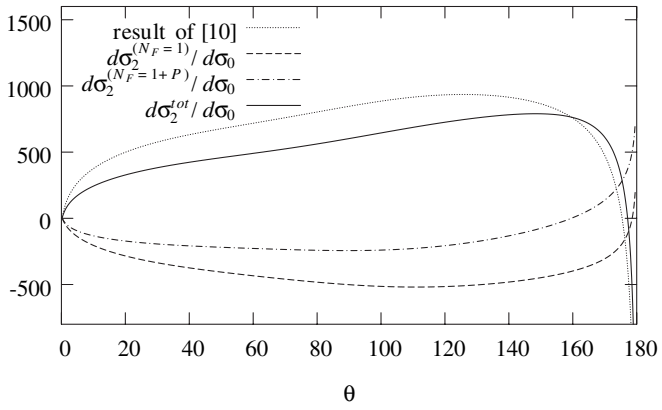

FIG. 18. Photonic, $N_F = 1$, and total contributions to the cross section at order α^4. E and ω as in Fig. 13. The pair production cutoff is set equal to ω.

tree-level amplitude and from the interference of one-loop box diagrams amongst themselves). Removing them from the vertex corrections, one obtains the dashed-dotted curve in Fig. 16, which is smoother than the dashed one. The solid curve represents the complete photonic cross section. As is already observed above, the vertex contribution reproduces the full result in the small-angle region.

The dashed line in Fig. 17 represents the quantity

$$\frac{d\sigma_2^{(\text{ph Boxes})}}{d\sigma_0} = \frac{d\sigma_2^{(\text{ph})}}{d\sigma_0} - \frac{d\sigma_2^{(\text{ph Vertices})}}{d\sigma_0} = \frac{d\sigma_2^{(\text{ph BoxBox})}}{d\sigma_0} + \frac{d\sigma_2^{(\text{ph 2L Box})}}{d\sigma_0}. \quad (90)$$

In the equation above, $\sigma_2^{(\text{ph BoxBox})}$ was introduced in Eq. (87), while $\sigma_2^{(\text{ph 2L Box})}$ is the contribution to the cross section of the two-loop photonic boxes interfered with the tree-level amplitude. The expression of the latter is given in Appendix B. Also in this case, the behavior at $\theta \sim 80°$ and at $\theta \sim 180°$ is dominated by the spurious terms of the kind of Eq. (89); by removing them, we obtain the dashed-dotted curve.

For completeness, in Fig. 18 we plot the photonic [10] and $N_F = 1$ [13] contributions to the Bhabha scattering cross section at order α^4. The dotted line represents the photonic corrections. The corrections of $\mathcal{O}(\alpha^4(N_F = 1))$ (dashed line) have, for this choice of ω ($\omega = E$), an opposite sign with respect to the photonic corrections. However, it is necessary to say that the $\mathcal{O}(\alpha^4(N_F = 1))$ of Ref. [13] include large contributions proportional to $\ln^3(s/m^2)$ that cancel out once the contribution of the soft-pair production is included. Of the latter, only the terms proportional to $\ln^n(s/m^2)$ ($n = 1, 2, 3$) are known (see [5]); we checked that they cancel the $\ln^3(s/m^2)$ term of the $\mathcal{O}(\alpha^4(N_F = 1))$ cross section. The dashed-dotted line represents the sum of the $\mathcal{O}(\alpha^4(N_F = 1))$ cross section with the known terms of the pair production corrections.[6] The solid line is the complete order α^4 QED Bhabha scattering cross section, including photonic, $N_F = 1$, and pair production contributions.

XI. CONCLUSIONS

In the present paper, we obtained analytic nonapproximated expressions for all of the photonic corrections to the QED Bhabha scattering differential cross section at second order [$\mathcal{O}(\alpha^4)$], except for the ones deriving from the interference of two-loop photonic box diagrams with the tree-level amplitude; at present, the integrals necessary to the calculation of the latter are not known. The calculations were carried out by retaining the full dependence on the electron mass m. The results are valid for arbitrary values of the c.m. energy s and momentum transfer t.

We included a discussion of the soft-photon emission at order α^4, employing dimensional regularization to handle the IR-divergent terms. We proved that the term proportional to $(D - 4)$ in the Laurent expansion of the photon phase-space integral I_{1j} in Eq. (62) does not contribute to the Bhabha scattering cross section.

After subtracting the IR singularities by adding the contribution of the soft-photon emission graphs, we expanded the contributions to the cross section discussed in Secs. III, IV, V, VI, and VII in the $m^2/s \to 0$ limit. In this way, it was possible to cross-check large parts of the result of Ref. [10], as well as to efficiently test our calculations. By subtracting the contributions to the cross section obtained in this paper from the cross section of Ref. [10], it was also possible to indirectly obtain the contribution due to the interference of the two-loop photonic diagrams with the tree-level amplitude, up to terms suppressed by positive powers of the electron mass.

By comparing the nonapproximated results with the corresponding $m^2/s \to 0$ limit, we explicitly checked that the contribution to the cross section of the terms proportional to positive powers of the ratio m^2/s is negligible at high- and intermediate-energy e^+e^- colliders. It is reasonable that the same conclusion applies to the contribution to the order α^4 cross section involving the two-loop photonic box diagrams. For what concerns phenomenological studies, the results of Refs. [6,10,12,13], therefore, provide a complete expression of the virtual and soft-photon emission corrections to the Bhabha scattering cross

[6]The pair production, calculated in Ref. [5] up to terms enhanced by $\ln^n(s/m^2)$ included, depends upon a cutoff on the energy of the soft electron-positron pair. In the numerical evaluation of Fig. 18 we set

$$\ln(\mathrm{D}) = \frac{1}{2}\ln\left(\frac{4\Omega^2}{s}\right), \quad (91)$$

with ln(D) defined in Ref. [5] and Ω numerically equal to the soft-photon cutoff: $\Omega = \omega$.

section at order α^4. To complete the study of the second order radiative corrections, it is still necessary to calculate the contribution of the soft-pair production up to terms not suppressed by m^2/s; at the moment, this class of corrections is known up to logarithmic terms [5]. Even if terms suppressed by positive powers of the electron mass are not phenomenologically relevant, a future calculation of the two-loop photonic box graphs for $m \neq 0$ would represent a very interesting result in the field of multiloop calculations.

ACKNOWLEDGMENTS

The authors thank H. Czyz, B. Tausk, and L. Trentadue for useful discussions and suggestions, as well as A. Penin for cross-checks, discussions, and for providing us with the expression of Eq. (3) of Ref. [10] in electronic format. We are grateful to J. Vermaseren for his kind assistance in the use of the algebra manipulating program FORM [28].

APPENDIX A: C_{ij} FUNCTIONS

In this appendix, we collect the explicit expressions of the c_{ij} functions employed in the main text:

$$c_{11}(s,t) = (s+t)^2 - 4m^2, \tag{A1}$$

$$c_{12}(s,t) = \tfrac{1}{2}[(s+t)^2 - st - 2m^2(s+t)], \tag{A2}$$

$$c_{13}(s,t) = 2(st - \tfrac{3}{2}tm^2 + \tfrac{3}{4}t^2), \tag{A3}$$

$$c_{14}(s,t) = -\tfrac{1}{4}st, \tag{A4}$$

$$c_{15}(s,t) = st + \frac{st^2}{4m^2} - 2tm^2 + \frac{3}{4}t^2 + \frac{t^3}{8m^2}, \tag{A5}$$

$$c_{16}(s,t) = \tfrac{1}{4}(st - 4tm^2 + 2t^2), \tag{A6}$$

$$c_{17}(s,t) = \frac{1}{4}st\left(1 + \frac{t}{m^2} + \frac{s}{m^2}\right), \tag{A7}$$

$$c_{21}(s,t) = 2\left[(s-2m^2)^2 + st + \frac{t^2}{2}\right], \tag{A8}$$

$$c_{22}(s,t) = \frac{t^2}{2}, \tag{A9}$$

$$c_{23}(s,t) = t(t+2m^2), \tag{A10}$$

$$c_{24}(s,t) = 0, \tag{A11}$$

$$c_{25}(s,t) = \frac{3t^2}{2}, \tag{A12}$$

$$c_{26}(s,t) = \frac{t^2}{2}, \tag{A13}$$

$$c_{27}(s,t) = st - \frac{st^2}{4m^2} - \frac{s^2t}{4m^2} + \frac{3}{4}t^2. \tag{A14}$$

APPENDIX B: TWO-LOOP PHOTONIC BOXES

We provide here the expansion of the interference of the two-loop photonic boxes with the tree-level amplitude in the limit $m^2/s \to 0$. Below one can find the contribution of the two-loop photonic boxes to the virtual cross section as well as the same contribution after the subtraction of the corresponding soft-photon corrections.

1. Two-loop photonic boxes before the inclusion of the soft radiation

$$\begin{aligned}\frac{d\sigma_2^{(V,\text{ph 2L Box})}}{d\sigma_0} = {} & \delta_{(2)}^{(V,\text{2L Box},3)} \log^3\left(\frac{s}{m^2}\right) \\ & + \delta_{(2)}^{(V,\text{2L Box},2)} \log^2\left(\frac{s}{m^2}\right) \\ & + \delta_{(2)}^{(V,\text{2L Box},1)} \log\left(\frac{s}{m^2}\right) \\ & + \delta_{(2)}^{(\text{2L Box},0)} + \mathcal{O}\left(\frac{m^2}{s}\right),\end{aligned} \tag{B1}$$

where

$$\delta_{(2)}^{(V,\text{2L Box},3)} = \frac{1}{(1-\xi+\xi^2)^2}\left\{-\left(\frac{7}{3} - \frac{14}{3}\xi + 7\xi^2 - \frac{14}{3}\xi^3 + \frac{7}{3}\xi^4\right)\ln(1-\xi) - \left(\frac{7}{6}\xi - \frac{7}{2}\xi^2 + \frac{7}{2}\xi^3 - \frac{7}{3}\xi^4\right)\ln(\xi)\right\}, \tag{B2}$$

$$\delta_{(2)}^{(V,\mathrm{2L\ Box},2)} = \frac{1}{(1-\xi+\xi^2)^2}\Bigg\{\frac{1}{(D-4)}[(-6+12\xi-18\xi^2+12\xi^3-6\xi^4)\ln(1-\xi)-(3\xi-9\xi^2+9\xi^3-6\xi^4)\ln(\xi)]$$
$$-\left(12-\frac{27}{2}\xi+\frac{63}{4}\xi^2-6\xi^3\right)\zeta(2)+\left(2-\frac{19}{4}\xi+\frac{27}{4}\xi^2-\frac{19}{4}\xi^3+2\xi^4\right)\ln^2(1-\xi)$$
$$+\left(\frac{11}{2}-\frac{29}{4}\xi+\frac{21}{2}\xi^2-\frac{29}{4}\xi^3+\frac{11}{2}\xi^4\right)\ln(1-\xi)-\left(7-14\xi+\frac{69}{4}\xi^2-\frac{19}{2}\xi^3+4\xi^4\right)\ln(\xi)\ln(1-\xi)$$
$$+\left(\frac{1}{2}\xi-\frac{21}{4}\xi^2+\frac{27}{4}\xi^3-\frac{11}{2}\xi^4\right)\ln(\xi)-\left(\frac{23}{8}\xi-\frac{45}{8}\xi^2+\frac{33}{8}\xi^3-2\xi^4\right)\ln^2(\xi)\Bigg\}, \tag{B3}$$

$$\delta_{(2)}^{(V,\mathrm{2L\ Box},1)} = \frac{1}{(1-\xi+\xi^2)^2}\Bigg\{\frac{1}{(D-4)^2}[-(8-16\xi+24\xi^2-16\xi^3+8\xi^4)\ln(1-\xi)-(4\xi-12\xi^2+12\xi^3-8\xi^4)\ln(\xi)]$$
$$+\frac{1}{(D-4)}\Bigg[(-24+30\xi-33\xi^2+12\xi^3)\zeta(2)+(10-15\xi+22\xi^2-15\xi^3+10\xi^4)\ln(1-\xi)$$
$$+(4-9\xi+13\xi^2-9\xi^3+4\xi^4)\ln^2(1-\xi)+(2\xi-11\xi^2+13\xi^3-10\xi^4)\ln(\xi)$$
$$-(12-24\xi+31\xi^2-18\xi^3+8\xi^4)\ln(\xi)\ln(1-\xi)-\left(\frac{9}{2}\xi-\frac{19}{2}\xi^2+\frac{15}{2}\xi^3-4\xi^4\right)\ln^2(\xi)\Bigg]$$
$$+\left(\frac{27}{2}\xi-\frac{33}{2}\xi^2+\frac{27}{2}\xi^3\right)\zeta(2)+\left(\frac{5}{2}\xi-4\xi^2+\frac{5}{2}\xi^3\right)+\left(12-38\xi+\frac{185}{2}\xi^2-89\xi^3+46\xi^4\right)\zeta(3)\zeta(2)$$
$$\times\ln(1-\xi)+\left(\frac{2}{3}\xi-\frac{1}{4}\xi^2+\frac{1}{6}\xi^3+\frac{1}{3}\xi^4\right)\ln^3(1-\xi)-\left(\frac{3}{2}\xi-\frac{5}{2}\xi^2+\frac{3}{2}\xi^3\right)\ln^2(1-\xi)$$
$$-(2-3\xi+3\xi^3-2\xi^4)\ln(1-\xi)\mathrm{Li}_2(\xi)-\left(12-\frac{67}{4}\xi+\frac{49}{2}\xi^2-\frac{67}{4}\xi^3+12\xi^4\right)\ln(1-\xi)$$
$$-\left(\xi-\frac{7}{2}\xi^2+4\xi^3-2\xi^4\right)\mathrm{Li}_3(1-\xi)+\left(2-4\xi+\frac{7}{2}\xi^2-\xi^3\right)\mathrm{Li}_3\left(-\frac{\xi}{(1-\xi)}\right)$$
$$-\left(2-\frac{5}{2}\xi+3\xi^2-\frac{5}{2}\xi^3+2\xi^4\right)\mathrm{Li}_3(\xi)-\left(24-\frac{57}{2}\xi+\frac{117}{2}\xi^2-\frac{123}{2}\xi^3+48\xi^4\right)\zeta(2)\ln(\xi)$$
$$+\left(3-\frac{15}{2}\xi+8\xi^2-\frac{9}{2}\xi^3+\xi^4\right)\ln(\xi)\ln^2(1-\xi)+\left(11-12\xi+8\xi^2+\frac{1}{2}\xi^3\right)\ln(\xi)\ln(1-\xi)$$
$$+\left(4-\frac{13}{2}\xi+\frac{13}{2}\xi^2-\frac{7}{2}\xi^3+2\xi^4\right)\ln(\xi)\mathrm{Li}_2(\xi)-\left(\frac{5}{4}\xi-\frac{49}{4}\xi^2+\frac{31}{2}\xi^3-12\xi^4\right)\ln(\xi)$$
$$-\left(5-\frac{49}{4}\xi+12\xi^2-\frac{13}{4}\xi^3-\xi^4\right)\ln^2(\xi)\ln(1-\xi)+\left(\frac{7}{8}\xi-\frac{5}{4}\xi^2+\frac{7}{8}\xi^3\right)\ln^2(\xi)$$
$$-\left(\frac{19}{6}\xi-\frac{25}{6}\xi^2+\frac{3}{2}\xi^3+\frac{1}{3}\xi^4\right)\ln^3(\xi)\Bigg\}, \tag{B4}$$

$$
\begin{aligned}
\delta_{(2)}^{(V,2\mathrm{L\ Box},0)} = {} & \frac{1}{(1-\xi+\xi^2)^2}\Bigg\{\frac{1}{(D-4)^2}[-(24-36\xi+36\xi^2-12\xi^3)\zeta(2)+(8-16\xi+24\xi^2-16\xi^3+8\xi^4) \\
& \times \ln(1-\xi)+(4-8\xi+12\xi^2-8\xi^3+4\xi^4)\ln^2(1-\xi)+(4\xi-12\xi^2+12\xi^3-8\xi^4)\ln(\xi) \\
& -(8-16\xi+24\xi^2-16\xi^3+8\xi^4)\ln(\xi)\ln(1-\xi)-(2\xi-6\xi^2+6\xi^3-4\xi^4)\ln^2(\xi)] \\
& +\frac{1}{(D-4)}\Bigg[(12\xi-15\xi^2+12\xi^3)\zeta(2)+(4-20\xi+69\xi^2-74\xi^3+40\xi^4)\zeta(2)\ln(1-\xi) \\
& -(8-11\xi+16\xi^2-11\xi^3+8\xi^4)\ln(1-\xi)-(2\xi-3\xi^2+2\xi^3)\ln^2(1-\xi)+(\xi-\xi^2+\xi^3) \\
& \times \ln^3(1-\xi)-(24-32\xi+57\xi^2-54\xi^3+40\xi^4)\zeta(2)\ln(\xi)-(\xi-8\xi^2+10\xi^3-8\xi^4)\ln(\xi) \\
& +(10-11\xi+8\xi^2)\ln(\xi)\ln(1-\xi)+(4-9\xi+8\xi^2-3\xi^3)\ln(\xi)\ln^2(1-\xi)+\left(\frac{1}{2}\xi-\frac{3}{2}\xi^2+\frac{1}{2}\xi^3\right) \\
& \times \ln^2(\xi)-\left(6-\frac{27}{2}\xi+\frac{27}{2}\xi^2-\frac{9}{2}\xi^3\right)\ln^2(\xi)\ln(1-\xi)-\left(\frac{5}{2}\xi-\frac{7}{2}\xi^2+\frac{3}{2}\xi^3\right)\ln^3(\xi)\Bigg] \\
& -\left(\frac{5}{2}\xi-\frac{21}{4}\xi^2+\frac{17}{2}\xi^3+3\xi^4\right)\zeta(2)+\left(12-\frac{149}{5}\xi+28\xi^2+\frac{39}{5}\xi^3-\frac{112}{5}\xi^4\right)\zeta^2(2) \\
& +\left(\xi-3\xi^2+\frac{3}{2}\xi^3\right)\zeta(3)-\left(11-\frac{43}{2}\xi+\frac{209}{4}\xi^2-57\xi^3+36\xi^4\right)\zeta(2)\ln(1-\xi) \\
& -\left(10-\frac{23}{2}\xi+9\xi^2-\frac{3}{2}\xi^3+4\xi^4\right)\zeta(3)\ln(1-\xi)-\left(21-\frac{73}{2}\xi+\frac{119}{4}\xi^2-7\xi^3+\xi^4\right)\zeta(2)\ln^2(1-\xi) \\
& -\left(\frac{1}{2}-\frac{29}{24}\xi+\frac{73}{48}\xi^2-\frac{5}{4}\xi^3+\frac{7}{12}\xi^4\right)\ln^4(1-\xi)-\left(\frac{1}{6}\xi-\frac{1}{6}\xi^2-\frac{1}{3}\xi^3+\frac{1}{3}\xi^4\right)\ln^3(1-\xi) \\
& +\left(5-\frac{15}{2}\xi+\frac{15}{2}\xi^3-5\xi^4\right)\ln^2(1-\xi)\mathrm{Li}_2(\xi)-\left(\frac{1}{2}-\frac{15}{4}\xi+\frac{9}{4}\xi^2-\frac{15}{4}\xi^3+\frac{1}{2}\xi^4\right)\ln^2(1-\xi) \\
& +\left(2-\frac{5}{2}\xi+\frac{5}{2}\xi^3-2\xi^4\right)\ln(1-\xi)\mathrm{Li}_2(\xi)+\left(6-9\xi-\frac{7}{2}\xi^2+14\xi^3-8\xi^4\right)\ln(1-\xi)\mathrm{Li}_3(1-\xi) \\
& -\left(2-4\xi+\frac{7}{2}\xi^2-\xi^3\right)\ln(1-\xi)\mathrm{Li}_3\left(-\frac{\xi}{(1-\xi)}\right)+\left(8-\frac{17}{2}\xi+4\xi^2+\frac{3}{2}\xi^3+2\xi^4\right)\ln(1-\xi)\mathrm{Li}_3(\xi) \\
& +\left(8-9\xi+\frac{29}{2}\xi^2-9\xi^3+8\xi^4\right)\ln(1-\xi)+(12\xi+17\xi^2-26\xi^3+38\xi^4)\zeta(2)\ln(\xi) \\
& +\left(6-\frac{5}{2}\xi+\xi^2-\frac{3}{2}\xi^3+4\xi^4\right)\zeta(3)\ln(\xi)+\left(40-\frac{115}{2}\xi+\frac{139}{2}\xi^2-\frac{113}{2}\xi^3+42\xi^4\right)\zeta(2)\ln(\xi)\ln(1-\xi) \\
& +\left(5-\frac{15}{2}\xi+\frac{5}{3}\xi^2+\frac{9}{2}\xi^3-\frac{8}{3}\xi^4\right)\ln(\xi)\ln^3(1-\xi)+\left(1-\frac{3}{4}\xi+\frac{1}{8}\xi^2+\frac{1}{4}\xi^3-\xi^4\right)\ln(\xi)\ln^2(1-\xi) \\
& -\left(12-\frac{33}{2}\xi+9\xi^2+\frac{3}{2}\xi^3\right)\ln(\xi)\ln(1-\xi)\mathrm{Li}_2(\xi)-\left(12-\frac{43}{4}\xi+10\xi^2+\frac{3}{2}\xi^3-\xi^4\right)\ln(\xi)\ln(1-\xi) \\
& -\left(12-\frac{45}{4}\xi+21\xi^2-\frac{101}{4}\xi^3+22\xi^4\right)\zeta(2)\ln^2(\xi)-\left(\frac{11}{2}-\frac{49}{8}\xi+\frac{5}{4}\xi^2+\frac{19}{8}\xi^3\right)\ln^2(\xi)\ln^2(1-\xi) \\
& +\left(\frac{7}{2}-6\xi+\frac{33}{8}\xi^2+\frac{1}{4}\xi^3-\xi^4\right)\ln^2(\xi)\ln(1-\xi)+\left(\frac{1}{3}+\frac{5}{4}\xi-\frac{11}{12}\xi^2-\frac{11}{12}\xi^3+\frac{5}{3}\xi^4\right)\ln^3(\xi)\ln(1-\xi) \\
& -\left(\frac{49}{48}\xi-\frac{17}{16}\xi^2+\frac{1}{12}\xi^3+\frac{5}{12}\xi^4\right)\ln^4(\xi)+\left(\frac{11}{6}\xi-\frac{25}{24}\xi^2+\frac{5}{24}\xi^3+\frac{1}{3}\xi^4\right)\ln^3(\xi) \\
& +\left(6-\frac{31}{4}\xi+\frac{31}{4}\xi^2-\frac{19}{4}\xi^3+3\xi^4\right)\ln^2(\xi)\mathrm{Li}_2(\xi)+\left(\frac{5}{4}\xi-\frac{11}{8}\xi^2+\frac{1}{4}\xi^3-\frac{1}{2}\xi^4\right)\ln^2(\xi) \\
& -\left(4-4\xi+\frac{3}{2}\xi^2-\frac{3}{2}\xi^3+2\xi^4\right)\ln(\xi)\mathrm{Li}_2(\xi)-\left(6-4\xi-\frac{13}{2}\xi^2+9\xi^3-2\xi^4\right)\ln(\xi)\mathrm{Li}_3(1-\xi)
\end{aligned}
$$

$$+\left(2-4\xi+\frac{7}{2}\xi^2-\xi^3\right)\ln(\xi)\mathrm{Li}_3\left(-\frac{\xi}{(1-\xi)}\right)-\left(6-\frac{3}{2}\xi+2\xi^2-\frac{9}{2}\xi^3+4\xi^4\right)\ln(\xi)\mathrm{Li}_3(\xi)$$
$$-\left(\xi+\frac{29}{4}\xi^2-10\xi^3+8\xi^4\right)\ln(\xi)+\left(22-31\xi+\frac{93}{2}\xi^2-44\xi^3+32\xi^4\right)\zeta(2)\mathrm{Li}_2(\xi)$$
$$+\left(\frac{3}{2}\xi-\frac{7}{2}\xi^2+\frac{7}{2}\xi^3-2\xi^4\right)\mathrm{Li}_3(1-\xi)-\left(2-4\xi+\frac{7}{2}\xi^2-\xi^3\right)\mathrm{Li}_3\left(-\frac{\xi}{(1-\xi)}\right)$$
$$+\left(2-2\xi^2-\frac{1}{2}\xi^3+2\xi^4\right)\mathrm{Li}_3(\xi)+\left(7\xi-\frac{9}{2}\xi^2-4\xi^3+6\xi^4\right)\mathrm{Li}_4(1-\xi)-\left(6-4\xi-\frac{9}{2}\xi^2+7\xi^3\right)$$
$$\times\mathrm{Li}_4\left(-\frac{\xi}{(1-\xi)}\right)-\left(2-\frac{17}{2}\xi+\frac{17}{2}\xi^3-2\xi^4\right)\mathrm{Li}_4(\xi)\Big\}. \tag{B5}$$

2. Two-loop photonic boxes after the inclusion of the soft radiation

$$\frac{d\sigma_2^{(\text{ph 2L Box})}}{d\sigma_0}=\delta_{(2)}^{(\text{2L Box},2)}\log^2\left(\frac{s}{m^2}\right)+\delta_{(2)}^{(\text{2L Box},1)}\log\left(\frac{s}{m^2}\right)+\delta_{(2)}^{(\text{2L Box},0)}+\mathcal{O}\left(\frac{m^2}{s}\right), \tag{B6}$$

where

$$\delta_{(2)}^{(\text{2L Box},2)}=\frac{1}{(1-\xi+\xi^2)^2}(-12+18\xi-18\xi^2+6\xi^3)\zeta(2), \tag{B7}$$

$$\delta_{(2)}^{(\text{2L Box},1)}=\frac{1}{(1-\xi+\xi^2)^2}\Big\{\frac{1}{(D-4)}(-24+36\xi-36\xi^2+12\xi^3)\zeta(2)+\ln^2\left(\frac{4\omega^2}{s}\right)[(-\xi+3\xi^2-3\xi^3+2\xi^4)\ln(\xi)$$
$$-(2-4\xi+6\xi^2-4\xi^3+2\xi^4)\ln(1-\xi)]+\ln\left(\frac{4\omega^2}{s}\right)\Big[\left(2\xi+\frac{3}{2}\xi^2-3\xi^3+2\xi^4\right)\zeta(2)$$
$$-\left(1-\frac{5}{2}\xi+\frac{7}{2}\xi^2-\frac{5}{2}\xi^3+\xi^4\right)\ln^2(1-\xi)-\left(3-\frac{11}{2}\xi+9\xi^2-\frac{11}{2}\xi^3+3\xi^4\right)\ln(1-\xi)$$
$$-(2-5\xi+9\xi^2-7\xi^3+4\xi^4)\mathrm{Li}_2(\xi)+\left(2-3\xi+\frac{1}{2}\xi^2+2\xi^3-2\xi^4\right)\ln(\xi)\ln(1-\xi)$$
$$-\left(\xi-\frac{9}{2}\xi^2+\frac{9}{2}\xi^3-3\xi^4\right)\ln(\xi)+\left(\frac{3}{4}\xi-\frac{1}{4}\xi^2-\frac{3}{4}\xi^3+\xi^4\right)\ln^2(\xi)\Big]+\left(9\xi-\frac{39}{4}\xi^2+\frac{15}{2}\xi^3+3\xi^4\right)\zeta(2)$$
$$-(12\xi-42\xi^2+48\xi^3-24\xi^4)\zeta(2)\ln(1-\xi)-\left(\frac{3}{2}-\frac{15}{4}\xi+\frac{21}{4}\xi^2-\frac{15}{4}\xi^3+\frac{3}{2}\xi^4\right)\ln^2(1-\xi)$$
$$-\left(\frac{3}{4}\xi+\frac{3}{4}\xi^3\right)\ln(1-\xi)-\left(3-\frac{15}{2}\xi+\frac{27}{2}\xi^2-\frac{21}{2}\xi^3+6\xi^4\right)\mathrm{Li}_2(\xi)-(24-30\xi+36\xi^2-30\xi^3$$
$$-24\xi^4)\zeta(2)\ln(\xi)+\left(3-\frac{9}{2}\xi+\frac{3}{4}\xi^2+3\xi^3-3\xi^4\right)\ln(\xi)\ln(1-\xi)+\frac{3}{4}\xi\ln(\xi)$$
$$+\left(\frac{9}{8}\xi-\frac{3}{8}\xi^2-\frac{9}{8}\xi^3+\frac{3}{2}\xi^4\right)\ln^2(\xi)\Big\}, \tag{B8}$$

$$
\begin{aligned}
\delta_{(2)}^{(2\mathrm{L\ Box},0)} = {} & \frac{1}{(1-\xi+\xi^2)^2}\Bigg\{\frac{1}{(D-4)^2}(-24+36\xi-36\xi^2+12\xi^3)\zeta(2)+\frac{1}{(D-4)}[(6\xi-12\xi^2+12\xi^3)\zeta(2) \\
& -(12\xi-42\xi^2+48\xi^3-24\xi^4)\zeta(2)\ln(1-\xi)-(24-30\xi+36\xi^2-30\xi^3+24\xi^4)\zeta(2)\ln(\xi)] \\
& +\ln^2\!\left(\frac{4\omega^2}{s}\right)\Bigg[(1-2\xi+3\xi^2-2\xi^3+\xi^4)\ln^2(1-\xi)+(2-4\xi+6\xi^2-4\xi^3+2\xi^4)\ln(1-\xi) \\
& -(2-4\xi+6\xi^2-4\xi^3+2\xi^4)\ln(\xi)\ln(1-\xi)+(\xi-3\xi^2+3\xi^3-2\xi^4)\ln(\xi) \\
& -\left(\frac{1}{2}\xi-\frac{3}{2}\xi^2+\frac{3}{2}\xi^3-\xi^4\right)\ln^2(\xi)\Bigg]+\ln\!\left(\frac{4\omega^2}{s}\right)\Bigg[\left(-2\xi-\frac{3}{2}\xi^2+3\xi^3-2\xi^4\right)\zeta(2) \\
& -\left(\frac{15}{2}\xi^2-9\xi^3+6\xi^4\right)\zeta(2)\ln(1-\xi)+\left(1-\frac{5}{2}\xi+\frac{7}{2}\xi^2-\frac{5}{2}\xi^3+\xi^4\right)\ln^3(1-\xi) \\
& +\left(1-2\xi+\frac{7}{2}\xi^2-2\xi^3+\xi^4\right)\ln^2(1-\xi)+(4-8\xi+12\xi^2-8\xi^3+4\xi^4)\ln(1-\xi)\mathrm{Li}_2(\xi) \\
& +\left(4-\frac{15}{2}\xi+12\xi^2-\frac{15}{2}\xi^3+4\xi^4\right)\ln(1-\xi)+(2-5\xi+9\xi^2-7\xi^3+4\xi^4)\mathrm{Li}_2(\xi) \\
& +\left(\frac{15}{2}\xi^2-9\xi^3+6\xi^4\right)\zeta(2)\ln(\xi)-\left(1-\frac{5}{2}\xi+\xi^2+\frac{1}{2}\xi^3-\xi^4\right)\ln(\xi)\ln^2(1-\xi) \\
& -\left(5-\frac{13}{2}\xi+5\xi^2+\xi^3-2\xi^4\right)\ln(\xi)\ln(1-\xi)-(2-5\xi+9\xi^2-7\xi^3+4\xi^4)\ln(\xi)\mathrm{Li}_2(\xi) \\
& +\left(\frac{3}{2}\xi-6\xi^2+6\xi^3-4\xi^4\right)\ln(\xi)+\left(2-\frac{15}{4}\xi+\frac{3}{4}\xi^2+\frac{11}{4}\xi^3-3\xi^4\right)\ln^2(\xi)\ln(1-\xi) \\
& -\left(\frac{1}{4}\xi-\frac{1}{4}\xi^2-\frac{3}{4}\xi^3+\xi^4\right)\ln^2(\xi)+\left(\frac{3}{4}\xi-\frac{1}{4}\xi^2-\frac{3}{4}\xi^3+\xi^4\right)\ln^3(\xi)\Bigg]+\left(\frac{7}{2}\xi-7\xi^2+4\xi^3\right)\zeta(3) \\
& -\left(\frac{1}{2}\xi+\frac{3}{2}\xi^2+\xi^3+7\xi^4\right)\zeta(2)+\left(12-\frac{353}{10}\xi+37\xi^2+\frac{3}{10}\xi^3-\frac{87}{5}\xi^4\right)\zeta^2(2) \\
& -\left(\frac{3}{2}\xi+17\xi^2-\frac{59}{2}\xi^3+18\xi^4\right)\zeta(2)\ln(1-\xi)-\left(13-18\xi+\frac{19}{2}\xi^2+4\xi^3-2\xi^4\right)\zeta(2)\ln^2(1-\xi) \\
& -\left(\frac{1}{4}-\frac{1}{8}\xi-\frac{11}{48}\xi^2+\frac{1}{3}\xi^3\right)\ln^4(1-\xi)+\frac{2}{3}\xi^2\ln^3(1-\xi)+\left(5-\frac{19}{2}\xi+7\xi^2-\frac{1}{2}\xi^3-\xi^4\right)\ln^2(1-\xi)\mathrm{Li}_2(\xi) \\
& +\left(\frac{3}{2}-\xi+4\xi^2-\xi^3+\frac{3}{2}\xi^4\right)\ln^2(1-\xi)+\left(\frac{3}{2}\xi+\frac{1}{2}\xi^3\right)\ln(1-\xi)\mathrm{Li}_2(\xi)+(6-10\xi+10\xi^3-6\xi^4) \\
& \times\ln(1-\xi)\mathrm{Li}_3(1-\xi)+(6-6\xi+\xi^2+4\xi^3)\ln(1-\xi)\mathrm{Li}_3(\xi)+(6\zeta(3)\xi+2\xi-\zeta(3)\xi^2-4\zeta(3)\xi^3 \\
& +2\xi^3-6\zeta(3))\ln(1-\xi)+\left(10\xi+\frac{25}{4}\xi^2-6\xi^3+18\xi^4\right)\zeta(2)\ln(\xi)+\left(28-36\xi+\frac{61}{2}\xi^2-23\xi^3+22\xi^4\right) \\
& \times\zeta(2)\ln(\xi)\ln(1-\xi)+\left(4-\frac{37}{6}\xi+\frac{8}{3}\xi^2+\frac{11}{6}\xi^3-\xi^4\right)\ln(\xi)\ln^3(1-\xi)-\left(\frac{3}{2}-4\xi+\frac{29}{8}\xi^2-\frac{3}{4}\xi^3\right) \\
& \times\ln(\xi)\ln^2(1-\xi)-\left(8-10\xi+\frac{1}{2}\xi^2+7\xi^3-4\xi^4\right)\ln(\xi)\ln(1-\xi)\mathrm{Li}_2(\xi) \\
& -\left(4-\frac{5}{4}\xi-2\xi^2+8\xi^3-5\xi^4\right)\ln(\xi)\ln(1-\xi)-\left(12-\frac{27}{2}\xi+14\xi^2-\frac{25}{2}\xi^3+11\xi^4\right)\zeta(2)\ln^2(\xi) \\
& -\left(\frac{11}{2}-\frac{27}{4}\xi+\frac{15}{8}\xi^2+2\xi^3-\frac{1}{2}\xi^4\right)\ln^2(\xi)\ln^2(1-\xi)+\left(3-\frac{15}{2}\xi+\frac{29}{4}\xi^2-2\xi^3\right)\ln^2(\xi)\ln(1-\xi) \\
& +\left(\frac{2}{3}-\frac{17}{12}\xi+\frac{3}{4}\xi^2+\frac{5}{12}\xi^3-\frac{2}{3}\xi^4\right)\ln^3(\xi)\ln(1-\xi)+\left(\frac{7}{48}\xi-\frac{5}{48}\xi^2-\frac{1}{12}\xi^3+\frac{1}{6}\xi^4\right)\ln^4(\xi) \\
& +\left(\frac{5}{3}\xi-\frac{3}{2}\xi^2+\frac{5}{24}\xi^3\right)\ln^3(\xi)+\left(2-\frac{11}{4}\xi+\frac{7}{4}\xi^2+\frac{1}{4}\xi^3-\xi^4\right)\ln^2(\xi)\mathrm{Li}_2(\xi)
\end{aligned}
$$

$$+\left(\xi-3\xi^2+\frac{13}{4}\xi^3-\frac{5}{2}\xi^4\right)\ln^2(\xi)-\left(3-\xi-\frac{1}{2}\xi^2+\frac{1}{2}\xi^3\right)\ln(\xi)\mathrm{Li}_2(\xi)-(6-5\xi-3\xi^2+5\xi^3)$$
$$\times\ln(\xi)\mathrm{Li}_3(1-\xi)-(4+\xi-\xi^2-2\xi^3+2\xi^4)\ln(\xi)\mathrm{Li}_3(\xi)-(3\zeta(3)\xi+2\xi+\zeta(3)\xi^2-2\zeta(3)\xi^3-6\zeta(3))\ln(\xi)$$
$$+\left(22-31\xi+\frac{63}{2}\xi^2-26\xi^3+20\xi^4\right)\zeta(2)\mathrm{Li}_2(\xi)+\left(3-\frac{13}{2}\xi+\frac{21}{2}\xi^2-\frac{15}{2}\xi^3+4\xi^4\right)\mathrm{Li}_2^2(\xi)$$
$$+(4-10\xi+18\xi^2-14\xi^3+8\xi^4)\mathrm{Li}_2(\xi)+\left(\frac{1}{2}\xi-\frac{1}{2}\xi^3\right)\mathrm{Li}_3(1-\xi)+\left(\frac{5}{2}\xi-5\xi^2+2\xi^3\right)\mathrm{Li}_3(\xi)$$
$$+\left(7\xi-\frac{9}{2}\xi^2-4\xi^3+6\xi^4\right)\mathrm{Li}_4(1-\xi)-\left(6-4\xi-\frac{9}{2}\xi^2+7\xi^3\right)\mathrm{Li}_4\left(-\frac{\xi}{(1-\xi)}\right)$$
$$-\left(2-\frac{17}{2}\xi+\frac{17}{2}\xi^3-2\xi^4\right)\mathrm{Li}_4(\xi)\Big\}. \tag{B9}$$

[1] S. Jadach *et al.*, hep-ph/9602393; G. Montagna, O. Nicrosini, and F. Piccinini, Riv. Nuovo Cimento **21N9**, 1 (1998).

[2] M. Consoli, Nucl. Phys. **B160**, 208 (1979); M. Bohm, A. Denner, and W. Hollik, Nucl. Phys. **B304**, 687 (1988).

[3] G. Faldt and P. Osland, Nucl. Phys. **B413**, 64 (1994); **B413**, 16 (1994); **B419**, 404(E) (1994); A. B. Arbuzov, E. A. Kuraev, and B. G. Shaikhatdenov, Mod. Phys. Lett. A **13**, 2305 (1998); A. B. Arbuzov, E. A. Kuraev, N. P. Merenkov, and L. Trentadue, Nucl. Phys. **B474**, 271 (1996).

[4] V. S. Fadin, E. A. Kuraev, L. Trentadue, L. N. Lipatov, and N. P. Merenkov, Yad. Fiz. **56N11**, 145 (1993) [Phys. At. Nucl. **56**, 1537 (1993)].

[5] A. B. Arbuzov, E. A. Kuraev, N. P. Merenkov, and L. Trentadue, Yad. Fiz. **60N4**, 673 (1997) [Phys. At. Nucl. **60**, 591 (1997)].

[6] E. W. N. Glover, J. B. Tausk, and J. J. Van der Bij, Phys. Lett. B **516**, 33 (2001).

[7] Z. Bern, L. J. Dixon, and A. Ghinculov, Phys. Rev. D **63**, 053007 (2001).

[8] R. Barbieri, J. A. Mignaco, and E. Remiddi, Nuovo Cimento Soc. Ital. Fis. A **11**, 824 (1972); **11**, 865 (1972).

[9] S. Catani, Phys. Lett. B **427**, 161 (1998).

[10] A. A. Penin, Phys. Rev. Lett. **95**, 010408 (2005).

[11] R. Bonciani, A. Ferroglia, P. Mastrolia, E. Remiddi, and J. J. van der Bij, Nucl. Phys. **B681**, 261 (2004); **B702**, 364(E) (2004).

[12] R. Bonciani, A. Ferroglia, P. Mastrolia, E. Remiddi, and J. J. van der Bij, Nucl. Phys. **B701**, 121 (2004).

[13] R. Bonciani, A. Ferroglia, P. Mastrolia, E. Remiddi, and J. J. van der Bij, Nucl. Phys. **B716**, 280 (2005).

[14] S. Laporta and E. Remiddi, Phys. Lett. B **379**, 283 (1996); S. Laporta, Int. J. Mod. Phys. A **15**, 5087 (2000).

[15] F. V. Tkachov, Phys. Lett. **100B**, 65 (1981); G. Chetyrkin and F. V. Tkachov, Nucl. Phys. **B192**, 159 (1981).

[16] T. Gehrmann and E. Remiddi, Nucl. Phys. **B580**, 485 (2000).

[17] A. V. Kotikov, Phys. Lett. B **254**, 158 (1991); **259**, 314 (1991); **267**, 123 (1991); E. Remiddi, Nuovo Cimento Soc. Ital. Fis. A **110**, 1435 (1997); M. Caffo, H. Czyz, S. Laporta, and E. Remiddi, Acta Phys. Pol. B **29**, 2627 (1998); Nuovo Cimento Soc. Ital. Fis. A **111**, 365 (1998).

[18] A. B. Goncharov, Math. Res. Lett. **5**, 497 (1998); D. J. Broadhurst, Eur. Phys. J. C **8**, 311 (1999); E. Remiddi and J. A. M. Vermaseren, Int. J. Mod. Phys. A **15**, 725 (2000); T. Gehrmann and E. Remiddi, Comput. Phys. Commun. **141**, 296 (2001); Nucl. Phys. **B601**, 248 (2001); **B640**, 379 (2002); Comput. Phys. Commun. **144**, 200 (2002).

[19] G. 't Hooft and M. J. G. Veltman, Nucl. Phys. **B44**, 189 (1972); C. G. Bollini and J. J. Giambiagi, Phys. Lett. **40B**, 566 (1972); Nuovo Cimento Soc. Ital. Fis. B **12**, 20 (1972); J. F. Ashmore, Lett. Nuovo Cimento Soc. Ital. Fis. **4**, 289 (1972); G. M. Cicuta and E. Montaldi, Lett. Nuovo Cimento Soc. Ital. Fis. **4**, 329 (1972); R. Gastmans and R. Meuldermans, Nucl. Phys. **B63**, 277 (1973).

[20] M. Czakon, J. Gluza, and T. Riemann, Nucl. Phys. B Proc. Suppl. **135**, 83 (2004).

[21] M. Czakon, J. Gluza, and T. Riemann, Phys. Rev. D **71**, 073009 (2005).

[22] V. A. Smirnov, Phys. Lett. B **524**, 129 (2002); G. Heinrich and V. A. Smirnov, Phys. Lett. B **598**, 55 (2004).

[23] J. Fleischer, T. Riemann, O. V. Tarasov, and A. Werthenbach, Nucl. Phys. B Proc. Suppl. **116**, 43 (2003).

[24] R. Bonciani, P. Mastrolia, and E. Remiddi, Nucl. Phys. **B661**, 289 (2003); **B702**, 359(E) (2004).

[25] R. Bonciani, P. Mastrolia, and E. Remiddi, Nucl. Phys. **B676**, 399 (2004).

[26] The expressions of the functions introduced in Secs. III, IV, V, and VI are included in the file Vfactors.inc; the expressions of the functions introduced in Sec. VII are included in the file Bfactors.inc. The expansions in the limit $m^2/s \to 0$ of all the contributions to the differential cross section discussed in the paper are collected in Expansions.inc. The files can be downloaded from pheno.physik.uni-freiburg.de/~bhabha.

[27] D. Bardin and G. Passarino, *The Standard Model in the Making: Precision Study of the Electroweak Interactions* (Oxford University, New York, 1999).

[28] J. A. M. Vermaseren, *Symbolic Manipulation with* FORM, Version 2 (Computer Algebra Nederland, Amsterdam, 1991); new features of FORM, math-ph/0010025.